

1 Reviewer-1

2 We appreciate your review and critique of the manuscript. Thank you.

3 Please note: Line numbers stated here are from the original manuscript.

4 The paper presents results from a measurement campaign (CCOPE) on the Chilean Pacific Coast. The  
5 data consist of particle number concentrations measured with a condensation particle counter (CPC)  
6 and size distributions measured with a high-resolution optical particle counter (UHSAS) at a  
7 measurement station near the town of Arauco. The data are used for parameterizations of aerosol  
8 properties relevant to cloud and precipitation processes: number-to-volume ratios, concentrations of  
9 cloud condensation nuclei and sea-salt aerosol. The goal is to use these parameterizations for  
10 interpreting other data collected during the campaign on the Nahuelbuta Mountains about 30 – 100  
11 km south of Arauco. The paper is basically well written and I can recommend its publication in ACP  
12 after some corrections and more detailed explanations.

13 It is in a way pleasant to see that it is still possible to make relevant observations even with such very  
14 simple traditional aerosol instrumentation when the setup in most similar campaigns today consists of  
15 several instruments measuring both physical properties and chemical composition. On the other hand,  
16 the lack of knowledge of size distributions at sizes smaller than those measured with the UHSAS,  
17 chemical composition and hygroscopicity increase the uncertainty of the interpretations. Discuss this.

18 We feel that the last four paragraphs of Section 4.4 address this. Please see Section 4.4 of the  
19 revised manuscript. Finally, since estimates of the effective supersaturation (Hudson 1984) are  
20 generally smaller than 0.2%, at least in liquid-only stratocumulus (Snider et al. 2017), we do not think  
21 that lack of knowledge at  $D < 0.06 \mu\text{m}$  is a limiting factor.

22 Hudson, J. G., 1984: Cloud condensation nuclei measurements within clouds. *J. Climate Appl.*  
23 *Meteor.*, 23, 42–51, doi:10.1175/1520-0450(1984)023,0042:CCNMWC.2.0.CO;2.

24 Snider, J.R., D.Leon and Z.Wang, Droplet Concentration and Spectral Broadening in Southeast  
25 Pacific Stratocumulus, *J. Atmos. Sci.*, 74, 719-749, 2017

26

27 The trajectories were calculated with HYSPLIT by using the GDAS wind data with a 0.5° spatial  
28 resolution. This is so coarse that the effects of local topography are not properly taken into account.  
29 The measurement site is very close to the town of Arauco and the sea, Gulf of Arauco is to the north of  
30 it and to the west of Arauco there are some hills higher than 300 m. As a result, even when the HYSPLIT  
31 trajectories show that wind blows from the west local wind in Arauco may have blown from other  
32 directions bringing anthropogenic aerosol from the town. The main goal of the paper is to use the  
33 parameterizations in the CCOPE data interpretations and modeling. During westerly winds the  
34 Nahuelbuta Mountains are definitely not affected by the anthropogenic sources around the Gulf of  
35 Arauco whereas your measurement station obviously is – the average total particle number  
36 concentration in air that you classified as "clean" was  $2759 \pm 1827 \text{ cm}^{-3}$ . This is high compared with  
37 marine aerosol essentially everywhere, possibly also on the coast directly to the west of the  
38 Nahuelbuta Mountains. In light of this, discuss the validity of the results for CCOPE.

39 Yes, spatial resolution of the GDAS is a factor limiting our ability to stratify measurements made  
40 at the Arauco Site. In spite of the limitation, our conditional sampling does demonstrate that aerosol  
41 surface area at the Arauco site is, on average, smaller than that reported by Hegg and Kaufman (1998)  
42 over the western Atlantic in air that had advected from the United States. The comparison of aerosol  
43 surface area is discussed in Sect. 5 of the manuscript. Related to your point about representativeness,  
44 the Arauco CPC data can be used to generate lower and upper quartile values of  $N_{\text{CPC}}$  ensemble. The  
45 quartiles are  $789$  and  $2151 \text{ cm}^{-3}$ , respectively. We did not present these  $N_{\text{CPC}}$  quartiles in the  
46 manuscript, but they are easily derived using the  $N_{\text{CPC}}$  ensemble described in the Supplementary  
47 Material (manuscript) or using the data reader we provided (see section titled "Data Availability"). The  
48 lower quartile  $N_{\text{CPC}}$  ( $789 \text{ cm}^{-3}$ ) indicates that 25% of the time conditions were comparable to the  
49 wintertime average at THD (Section 4.1).

50 You also assert that "...directly west of Nahuelbuta Mountains.." a more pristine aerosol state  
51 may exist. We are not convinced this is true. In Fig. 1 (revised manuscript), Lebu (population 24,000)  
52 and Cañete (population 32,000) are included. Another small city (Curanilahue) was in Figure 1 of the  
53 original manuscript. These small cities increase the possibility that cloud and precipitation over the  
54 Nahuelbuta are impacted by anthropogenic aerosols, even in a westerly flowing air. Furthermore,  
55 source/receptor relationships for aerosols on the Central Chilean Coast depend on source strength and

56 a host of meteorological factors (e.g., extratropical cyclone track, thermal stability, and etc.).  
57 Onshore/offshore flow that occurs during meteorologically quiescent periods (sea/land breeze  
58 circulations), could also be significant. For example, if the sea/land circulation creates a “strip” of  
59 aerosol contamination within the near-shore zone, and this air is brought onshore during episodes of  
60 persistent westerly airflow. A “coastal strip” of larger cloud droplet concentration is evident in analyses  
61 of satellite retrievals in Wood et al. (2012; their figure 4). The latter compliments the retrievals of  
62 Bennartz (2007), who we cite in the manuscript (Sect. 5). However, neither Wood et al. (2012) nor  
63 Bennartz (2007) segregate the satellite data into wintertime and summertime ensembles. As we state  
64 in the manuscript (Sect. 5), further analysis of the satellite retrievals are needed to investigate if the  
65 coastal strip exists both in winter and in summer.

66 The previous paragraph focused on aerosol-cloud interactions occurring within the planetary  
67 boundary layer; an additional dimension of the problem is aerosol resident above the planetary  
68 boundary layer. We acknowledge this in Sect. 5 (original and revised manuscript).

69 In summary, we feel that the caveats provided in the manuscript (Sections 5 and 6) are  
70 sufficient for numerical modelling of wintertime Chilean Coastal clouds and precipitation. We are  
71 confident that such modelling will extend understanding beyond the analyses provided here and in  
72 Massmann et al. (2017).

73 Hegg, D. A., and Y. J. Kaufman, Measurements of the relationship between submicron aerosol  
74 number and volume concentration, *J. Geophys. Res.*, 103, 5671-5678, 1998

75 Massmann, A.K., J.R. Minder, R.D. Garreaud, D.E. Kingsmill, R.A. Valenzuela, A. Montecinos, S.L.  
76 Fults, and J.R. Snider, 2017, The Chilean Coastal Orographic Precipitation Experiment: Observing the  
77 Influence of Microphysical Rain Regimes on Coastal Orographic Precipitation. *J. Hydrometeor.*, 18,  
78 2723–2743, <https://doi.org/10.1175/JHM-D-17-0005.1>, 2017

79 Bennartz, R., Global assessment of marine boundary layer cloud droplet number concentration  
80 from satellite, *J. Geophys. Res.*, 112, D02201, 2007

81 Wood, R. ( 2006), Rate of loss of cloud droplets by coalescence in warm clouds, *J.*  
82 *Geophys. Res.*, 111, D21205, doi:10.1029/2006JD007553.

84 **Detailed comments**

85 Section 2.1. Add information on the distance of the Arauco measurement site from the sea, from the  
86 town of Arauco, the paper mill, the Curanilahue measurement station and the rest of the CCOPE  
87 campaign area.

88 A distance scale is provided in Fig. 1 (revised manuscript). Also, a city Coronel (population  
89 110,000), and two small cities Lebu (population 24,000) and Cañete (population 32,000) are included in  
90 the revised Fig. 1.

91 L145-146 " ... CPC concentrations were recorded once per second and once every 10 seconds (Table 1)."

92 The expression "CPC concentrations" would mean there are many Condensation Particle Counters  
93 flying in the air. That is not quite correct. Use "... CPC data were recorded..."

94 **Corrected**

95 Another thing I don't understand, is the logic of saving data once per s and once per 10 s. The 1-s data  
96 has it all, from it 10-s data can be picked up if needed. What is the logic?

97 **The text was revised:**

98 "The CPC counts particles larger than  $D = 0.010 \mu\text{m}$  (Table 1) up to a maximum concentration of 10,000  
99  $\text{cm}^{-3}$ . The UHSAS measures scattering produced when aerosol particles are drawn through light  
100 emitted by a solid state laser ( $\lambda = 1.05 \mu\text{m}$ ). By reference to a calibration table (Cai et al. 2008; Cai et al.  
101 2013), the UHSAS microprocessor converts scattered light intensity to particle size and accumulates  
102 the derived sizes in a 99 channel histogram. Channel widths are logarithmically uniform ( $\Delta\log_{10}D =$   
103 0.013) over the instrument's full range ( $0.055 < D < 1.0 \mu\text{m}$ ). UHSAS data were recorded every 10  
104 seconds and CPC data were recorded once per second (Table 1)."

105 The expressions "**CPC concentration**" and "**UHSAS concentration**" have been used in some sentences  
106 also later. As I wrote above, these should be rewritten. For example title of section 4.1 should rather  
107 be "Comparison of particle number concentrations..."

108 **Corrected.**

109 L256-258 " ... 194 classify as clean sector. For both sites we required a clean sector wind speed  $> 1.5 \text{ m}$   
110  $\text{s}^{-1}$  in addition to the clean sector directional criteria (Fig. 2)."

111 You started wind measurements at Arauco on 19 June. Did you use only the aerosol data after that in  
112 this comparison?

113 **Yes.**

114 L286-289 " ***During this two-hour data segment, centered on 00 UTC June 9 (9 pm local time), winds were light at***  
115 ***Arauco and Curanilahue ( $< 2 \text{ m s}^{-1}$ ) and the wind direction was variable at Curanilahue (Arauco Site wind direction***  
116 ***measurements are only available after 19 June 2015; Sect. 2.1).***"

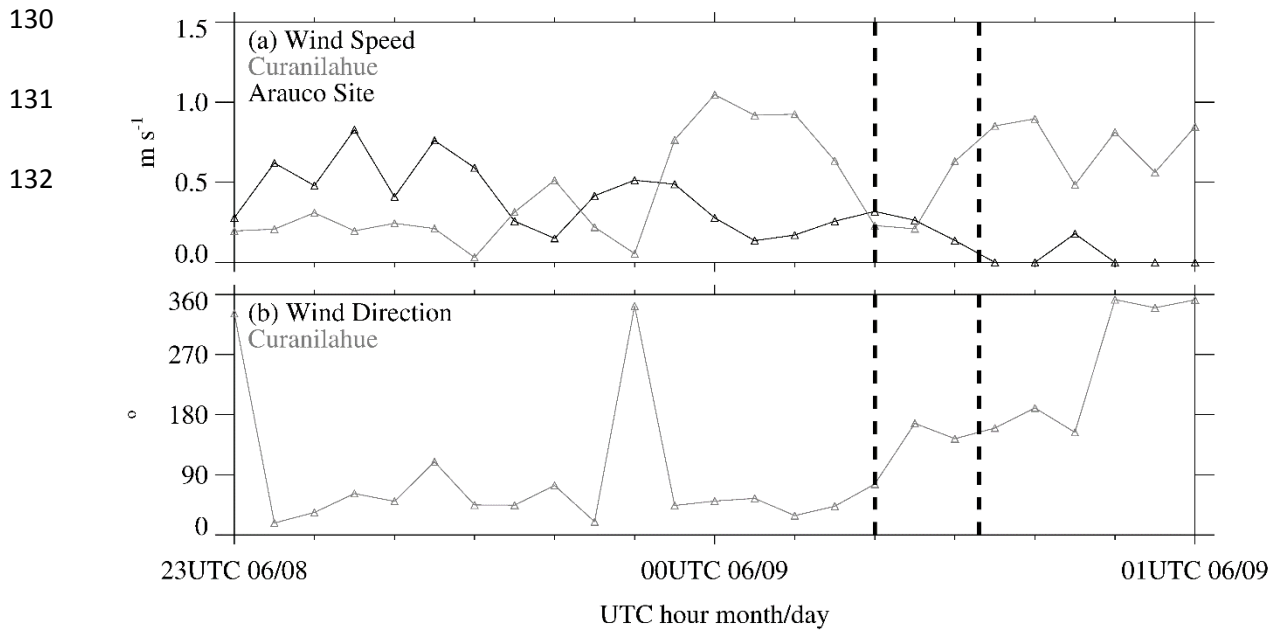
117 You wrote that wind measurements at Arauco started on 19 June. How can you then write that the  
118 wind at Arauco was  $< 2 \text{ m/s}$  on 9 June?

119 **Meteorological measurements (minus wind direction) were acquired from 29 May to 14 August**  
120 **and meteorological measurements (including wind direction) were acquired 19 June to 14 August. This**  
121 **is stated in Section 2.1 (original and revised manuscript).**

122

123 The distance between Arauco and Curanilahue is approximately 25 km, the measurement site of  
124 Curanilahue is at > 100 m ASL and there are quite a few valleys and hills higher than 100 m ASL between  
125 the two sites. So the local winds at these sites may have been completely different. How justifiable is it  
126 to use Curanilahue in interpreting Arauco data?

127 **Reviewer #1 also commented on this, and we responded. Wind speeds were light at both**  
128 **locations and direction was variable at Curanilahue. A graph of the data is provided below. In general,**  
129 **the effect of wind on aerosol is very difficult to interpret.**



133 Section 4.3

134 In calculating the  $N/V$  ratio, justify using  $N_{UHSAS}$  and not  $N_{CPC}$  for  $N$ ?

135 We rewrote this section of the manuscript. We feel the revision justifies what you commented  
136 on:

137 “In this section we analyze two ASD moments (Section 3.3). These are symbolized  $N_{UHSAS}$  and  $V_{UHSAS}$ ,  
138 respectively. The ratio of  $N_{UHSAS}$  (aerosol concentration) and  $V_{UHSAS}$  (aerosol volume) – generically the  
139  $N/V$  ratio - is of interest for several reasons. First, for both operational and theoretical reasons the  $N/V$   
140 ratio is evaluated for particle diameters larger than  $\sim 0.1 \mu\text{m}$  (VD00; Hegg and Kaufman 1998, hereafter  
141 HK98), and importantly, the model developed to evaluate aerosol exchange between an overlying free  
142 troposphere (FT) and the marine boundary layer (MBL) successfully predicts the  $N/V$  ratio in the MBL  
143 (VD00). Second, a value of the ratio can be derived by fitting measurements of  $N$  and  $V$  (HK98). Third,  
144 aerosol mass loading, and thus an aerosol volume corresponding to an assumed particle density<sup>1</sup>, are  
145 relatively easy to evaluate. A method routinely used to evaluate aerosol mass loading involves pulling  
146 aerosol-laden air through a filter and evaluating the accumulated mass gravimetrically. Fourth, the  
147 product of an  $N/V$  ratio and an ambient aerosol volume (aerosol mass) has been proposed as a scheme  
148 for estimating cloud droplet concentration in marine stratocumulus clouds (HK98 and VD00).  
149 HK98 used a passive cavity aerosol spectrometer probe (PCASP) to evaluate  $N$ ,  $V$  and the  $N/V$  ratio.  
150 Since the UHSAS counts down to a smaller diameter ( $0.055 \mu\text{m}$ ) than the PCASP ( $0.12 \mu\text{m}$ ), it is  
151 expected that the  $N/V$  ratios we derive using the UHSAS will be larger than those in HK98. The main  
152 reason for this is that decreasing the lower-limit diameter increases  $N$  more than  $V$  (VD00).”

153 Hegg, D. A., and Y. J. Kaufman, Measurements of the relationship between submicron aerosol  
154 number and volume concentration, *J. Geophys. Res.*, 103, 5671-5678, 1998

155 van Dingenen, R., A. O. Virkkula, F. Raes, T. S. Bates, A. Wiedensohler, A simple non linear  
156 analytical relationship between aerosol accumulation number and sub-micron volume, explaining their  
157 observed ratio in the clean and polluted marine boundary layer, *Tellus*, 52B, 439-451, 2000

158 \_\_\_\_\_  
<sup>1</sup> In the case of ambient particles containing hygroscopic materials, density values range between  $1.5$  and  $1.8 \text{ g cm}^{-3}$   
(McMurry et al. 2002)

159 What did HK98 and VD00 use?

160 This information is provided in Sect. 4.3. First we present  $N/V$  ratios derived with the lower-  
161 limit diameter set at the minimum particle diameter detected by the UHSAS. Next, we repeat the  
162 analysis with the lower-limit diameter equal to the value applied by HK98. Results are in Tables 3 and  
163 4. The “headline” of these Tables provides the distinction. Additionally, VD00 integrate from minimum  
164 diameter = 0.08  $\mu\text{m}$ , but we do not consider that case.

165



166 Section 4.4

167 L377-385 This is an important part of the paper and it should be understood properly in order to  
168 understand the parameterization FAC(SS) presented later. Now it is not quite clear to me. You have  
169 earlier presented some of the simplest possible aerosol equations, Eqs. (1) – (4), which is fine, they are  
170 good to be shown. But now when it comes to a clearly more complicated issue, equations are missing  
171 which is not logical. And on line 379 it is written " ... **kappa–Köhler formula of Petters and Kreidenweis**  
172 **(2007, their Eq. (11))**" but their Eq. (11) shows the relationship of growth factor, dry particle diameter,  
173 kappa, and relative humidity. How is this used to "...interpret a FAC's lower-limit diameter as an upper-limit  
174 SS" as was stated on line 377? Is the referred equation right? Write the proper equation and explain the steps of  
175 the calculation in more detail so that readers can repeat the calculation for their own data.

176 The relevant equation from Petters and Kreidenweis (2007) was cited incorrectly. This is  
177 changed in the revised manuscript. For calculating critical SS, corresponding to prescribed values of dry  
178 diameter and kappa, we used Eq. 6 (Petters and Kreidenweis 2007). This is corrected in the revised  
179 manuscript. Additionally, our explanation is enhanced by inclusion of Eq. 5 (revision).

180 Here is the revised text:

181 "Our first step is to select a particle diameter, apply this as a lower-limit diameter in an integration of  
182 the UHSAS size distribution, and divide the integral by the coincident CPC-measured concentration.  
183 The resultant is referred to as the *fractional aerosol concentration (FAC)*.

184 
$$FAC(D) = \frac{1}{N_{CPC}} \cdot \int_D^{1\mu m} (dN / d \log_{10} D) \cdot d \log_{10} D \quad (5)$$

185 Figs. 7a - b have graphical representations of  $FAC(D=0.055 \mu m)$  and  $FAC(D=0.120 \mu m)$ .

186 In a second step we interpret a FAC's lower-limit diameter as an upper-limit SS. We do this by applying  
187 a value for the kappa hygroscopicity parameter, which we set at  $\kappa = 0.5$ , and by applying the kappa–  
188 Köhler formula of Petters and Kreidenweis (2007, their Eq. (6)). This transformation from lower-limit  $D$   
189 to upper-limit SS converts the FAC in Fig. 7a to  $FAC(SS = 0.41 \%)$  and the FAC in Fig. 7b to  $FAC(SS = 0.13$   
190  $\%)$ . We also evaluated how a range of the kappa parameter ( $0.3 < \kappa < 0.7$ ) translates to a range of SS.  
191 Our upper-limit  $\kappa$  comes from airborne measurements made over the Southeast Pacific Ocean during

192 summer (Snider et al., 2017), and our lower-limit  $\kappa$  is the value recommended by Andreae and  
193 Rosenfeld (2008) for simulating aerosol indirect effects over continents.”

194

195 Additionally, we rewrote the paragraph explaining how FACs are derived for onshore trajectories. The  
196 revised paragraph is this:

197

198 “The *FACs* in Figs. 7a – b are two of the many available from CCOPE. One way to aggregate these is to  
199 calculate a *FAC* for each of the 20 onshore trajectories. For example, if we select the lower-limit  
200 diameter at  $D = 0.055 \mu\text{m}$ , plot numerator values (Eq. (5)) vs denominator values (Eq. (5)), and fit with  
201 the equation  $Y = a \cdot X$ , the “ $a$ ” we derive is the  $FAC(D = 0.055 \mu\text{m})$  for a particular trajectory. *FACs*  
202 calculated in this way, and with lower-limit  $D$  selected =  $0.120 \mu\text{m}$ , are presented in the seventh  
203 columns of Tables 3 and 4. Correlation coefficients presented in the eighth columns of these tables  
204 mostly exceed 0.5. By averaging over the 20 onshore trajectories, we calculated the overall averages  
205 presented at the bottom of the two tables. These overall averages are  $FAC(D = 0.055 \mu\text{m}) = 0.35 \pm 0.13$   
206 (Table 3) and  $FAC(D = 0.120 \mu\text{m}) = 0.13 \pm 0.07$  (Table 4). This decrease of the *FAC* results because a  
207 larger lower-limit  $D$  (Eq. (5)), implies a smaller numerator (Eq. (5)), and thus a smaller  $FAC(D)$ .”

208

209

210 Section 4.5

211 Refer also to O’Dowd, C. D. and de Leeuw, G. (2007) and consider comparing your results also with the  
212 parameterization they presented

213 O’Dowd, C. D. and de Leeuw, G.: Marine Aerosol Production: a review of the current knowledge, Phil.  
214 Trans. R. Soc. A., 365,1753–1774, doi:10.1098/rsta.2007.2043, 2007

215 O’Dowd and de Leeuw (2007) summarize the sea spray research of Geever et al. (2005) and  
216 Clarke et al. (2006). The latter two references are not compiled in Lewis and Schwartz (2004) (hereafter  
217 LS04). We reference LS04 and Clarke et al. (2006) in the manuscript (original and revised).

218 Clarke et al. (2006) report a particle size-dependent flux function. As discussed in de Leeuw et  
219 al. (2011) (their section 6.5), a *size-dependent flux* can be transformed to a *concentration*,  
220 corresponding to a specified range of particle size, but this requires a steady-state, an assumed value  
221 for atmospheric residence time, and an assumed value for the depth of the MBL. Geever et al. (2005)  
222 investigated sea spray from particles smaller than 1  $\mu\text{m}$ , but did not report a size-dependent flux  
223 function.

224 Using the Clarke et al. (2006) parameterization with a range of wind speeds (3, 6, and 12 m/s),  
225 we transformed to concentrations assuming residence time = 3 day and MBL depth = 500 m (de Leeuw  
226 et al. (2011); their section 6.5). The SSA concentrations we calculated are within a factor = 3 of the  
227 CCOPE curve in Fig. 9. Specifically, the calculated values are smaller at 3 m/s (Fig.9-to-calculated ratio =  
228 1.3) and larger at 12 m/s (Fig.9-to-calculated ratio = 0.33). Given that there is significant variability in  
229 residence time and MBL depth, and in the wind speed scaling applied in Clarke et al. (2006), the result  
230 in Fig. 9 (manuscript) seems reasonable.

231 Summary: Because of assumptions necessary to transform a size-dependent flux to a  
232 concentration, we have not compared our result to sea spray research other than the comparison to  
233 wind-speed-dependent concentrations presented in O’Dowd and Smith (1993).

234 Clarke, A., V. Kapustin, S. Howell, K. Moore, B. Lienert, S. Masonis, T. Anderson, and D. Covert,  
235 Sea-salt size distribution from breaking waves: Implications for marine aerosol production and optical  
236 extinction measurements during SEAS, J. Atmos. Ocean. Technol., 20, 1362–1374, 2003

237            Geever, M., C. D. O'Dowd, S. van Ekeren, R. Flanagan, E. D. Nilsson, G. de Leeuw, and Ü. Rannik,  
238            Submicron sea spray fluxes, *Geophys. Res. Lett.*, 32, L15810, doi:10.1029/2005GL023081, 2005

239            de Leeuw, G., E. L. Andreas, M. D. Anguelova, C. W. Fairall, E. R. Lewis, C. O'Dowd, M. Schulz,  
240            and S. E. Schwartz, Production flux of sea spray aerosol, *Rev. Geophys.*, 49, RG2001,  
241            doi:10.1029/2010RG000349, 2011

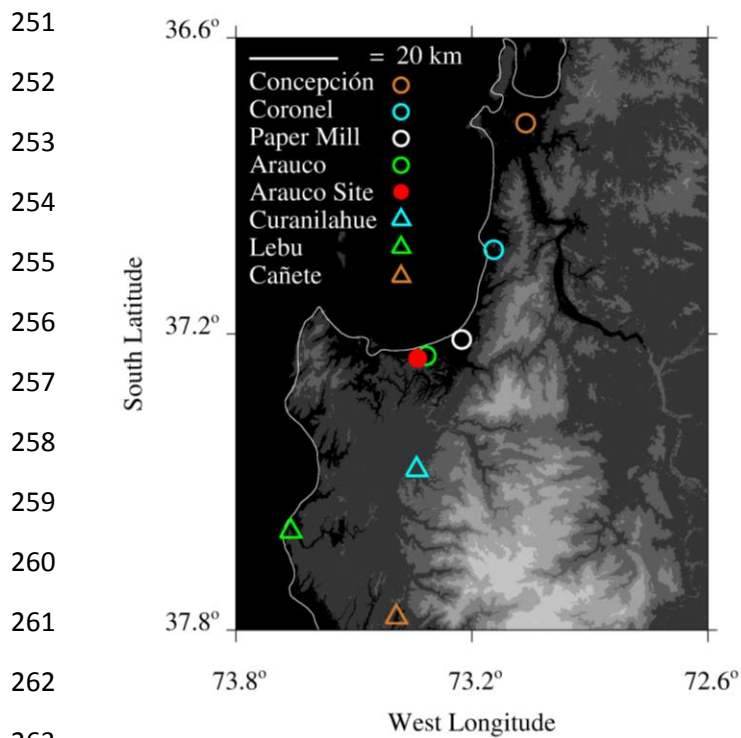
242            O'Dowd, C. and G. de Leeuw, Marine aerosol production: a review of the current knowledge,  
243            *Phil. Trans. R. Soc. A.*, 365, 1753–1774, doi:10.1098/rsta.2007.2043, 2007

244            O'Dowd, C.D., and M.H. Smith, Physicochemical properties of aerosols over the Northeast  
245            Atlantic: evidence for wind-speed-related submicron sea-salt aerosol production, *J. Geophys. Res.*, 98,  
246            1137-1149, 1993

247

248 Fig 1. Add a distance scale.

249 Fig. 1 (revised manuscript) has a distance scale. The revised map is shown below. Small cities  
250 Cañete and Lebu, and the city Coronel, are included in the revised Figure 1.

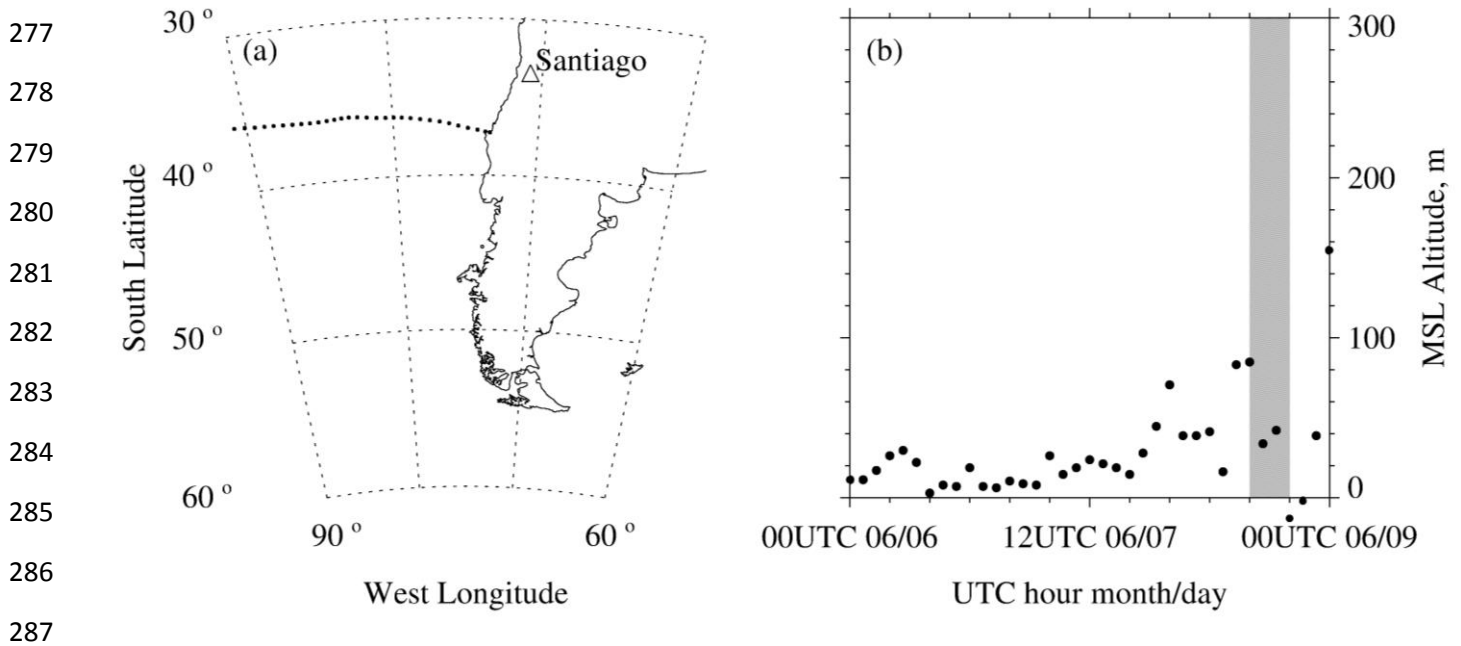


266 Fig. 3b. Why is the y axis reverse? Why is the lowest pressure 920 hPa? A sensible scale would be 990-  
267 1020 hPa.

268 An air parcel's barometric pressure is output by the HYSPLIT model. Fig. 3b (original manuscript)  
269 has this pressure on the Y axis. Pressure, decreasing upward on the Y axis, is a proxy for altitude. In the  
270 revised Fig. 3b (see below), the MSL altitude of the air parcel is plotted. MSL altitude was calculated  
271 using the pressure output by HYSPLIT (parcel barometric pressure) and the ICAO equation for the  
272 Standard Atmosphere (1993). MSL altitude increases if a larger sea-level is pressure applied in the ICAO  
273 equation. This sensitivity is  $\sim 8 \text{ m} / \text{hPa}$ .

274 International Civil Aviation Organization (ICAO), Manual of the ICAO Standard Atmosphere:  
275 extended to 80 kilometres (262500 feet), 3rd ed., ISBN-92-9194-004-6, 1993

276



288 Fig. B1. What is the vertical dashed line at ~11:33 UTC?

289 This is explained in the original manuscript (Appendix B). Readers are referred to Appendix B at  
290 L194. The first paragraph of Appendix B (revised manuscript) was revised for clarity. Here is the  
291 revised text:

292 “For each of the onshore trajectories (Sect. 3.1), a two-hour segment, centered on the trajectory arrival  
293 time was analyzed. An example is in Figs. B1a – e. The first panel (Fig. B1a) shows the sequence of  
294 CPC values sampled every second (i.e., 1-s samples referred to as *fast*  $N_{CPC}$ ), and Fig. B1b shows CPC  
295 values sampled every 10 seconds (i.e., 10-s samples referred to as *slow*  $N_{CPC}$ ). The following procedure  
296 was used to attenuate the narrow perturbations that were likely the result of local aerosol emissions (e.g.,  
297 within the time interval indicated by vertical dashed lines in Figs. B1a, B1b, and B1d).”

1 Reviewer-2

2 We appreciate your review and critique of the manuscript. Thank you.

3 Please note: Line numbers stated here are from the original manuscript.

4 **General Comments:**

5 The paper describes aerosol data obtained in a 3-month observational study at a coastal site in  
6 Chile. Aerosol observations in this part of the world are rare so the data should be of interest to  
7 the community. Hence, I support publication of this work.

8 I offer some comments below that the authors can consider in revision. In general, I think some of  
9 the discussion of standard instruments and approaches could be stream-lined or moved to the  
10 Appendix.

11 The analyses and findings are fairly straightforward. Implications could be strengthened by  
12 additional comparison to observations that are clearly “clean marine”.

13 This was addressed by revising the final sentences of Section 4.1:

14 “These averages are also statistically different ( $p < 0.01$ ), and again, the Arauco average is larger  
15 than that at THD. Based on averages presented in this section, and information provided in Table  
16 2, two summary statements are warranted: 1) During wintertime, the THD classifies as a  
17 moderately-polluted marine site, and the Arauco Site classifies between moderately-polluted  
18 marine and heavily-polluted marine. 2) These sites are not representative of conditions well  
19 removed from anthropogenic influence.”



20 **Specific Comments:**

21 Line 52: it's not clear how these aerosol indirect effects differ, as described here; please clarify. The  
22 Albrecht reference may refer to hypothesized increasing cloud lifetime and cloud cover due to  
23 increased aerosol?

24 **We revised this:**

25 **“Consequently, upward reflection of solar radiation by liquid-only clouds (Twomey 1974), and upward**  
26 **reflection attributable to cloud fractional coverage (Albrecht 1989), increase with increased aerosol**  
27 **abundance.”**

28 Line 61: perhaps the VOCALS study should be cited as a contribution to Southern Hemisphere field  
29 work exploring aerosol-cloud interactions.

30 The references we picked contrast Southern and Northern Hemisphere aerosol and cloud  
31 properties. We are not aware of a VOCALS-related publication that does that. There is reference  
32 to VOCALS in Sections 4.4 (Snider et al. 2017; manuscript bibliography).

33 Line 70: I think you mean that the presence of SSA is associated with the presence of giant CCN that  
34 promote drizzle production.

35 We do not use the modifier “giant” when referring to a subclass of the aerosol. We did change  
36 the text to stress that most of the CCN are smaller than the class of SSA particles ( $D > 0.5 \mu\text{m}$ ) that we  
37 focus on. Here is how the paragraph is rewritten:

38 “We emphasize the following topics: 1) The parameterized relationship between sea salt aerosol (SSA)  
39 particles (diameter  $> 0.5 \mu\text{m}$ ) and wind speed; 2) The role as cloud condensation nuclei (CCN) of  
40 particles that are both smaller and more numerous than the above-mentioned SSA; 3) The  
41 parameterized relationship describing CCN activation spectra (Rogers and Yau, 1989; chapter 6), and 4)  
42 the potential application of the SSA and CCN parameterizations in numerical modelling of wintertime  
43 Southern Hemispheric clouds and precipitation. Motivating our investigation are modeling studies  
44 (Feingold et al. 1999), and analyses of field measurements (Gerber and Frick 2012), indicating that the  
45 reduction of rainfall due to increased CCN can be negated by SSA particles.”

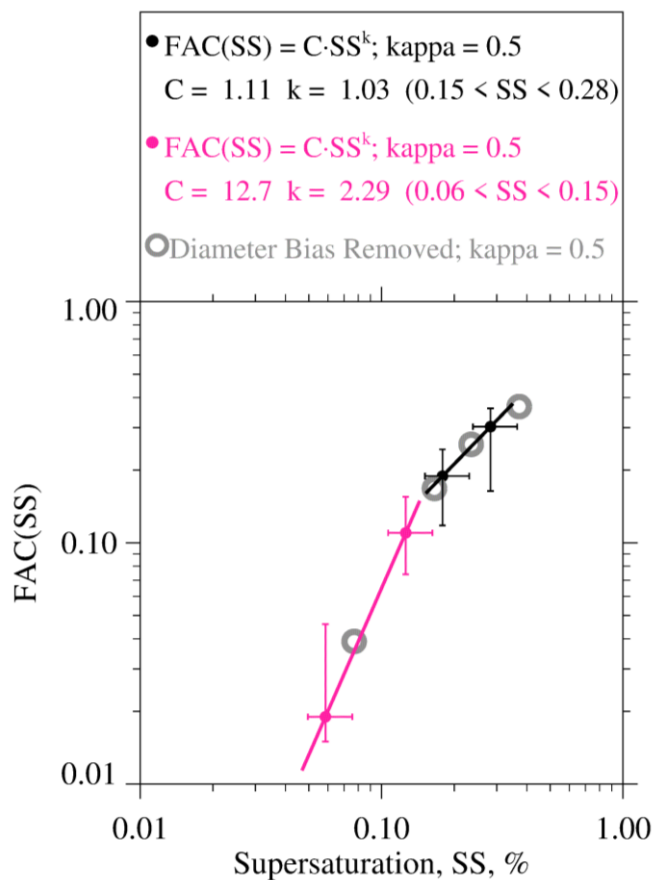
46

47

48 Line 132: the particle size overestimate due to not being fully dried is discussed and a ballpark %  
49 given. However, it seems the data were not corrected for this. The CCN estimate will therefore be  
50 affected since critical supersaturation is very sensitive to size. Why wasn't this factored in? (Since a  
51 kappa is assumed, the data could be corrected for water content if RH is known.) Could this  
52 overestimate be used to add uncertainties into the parameterization?

53 Our analysis of the 20% particle-size overestimate is in the figure below. The pink and black  
54 data points, and their uncertainties and fit lines, are replicated from Fig. 8 (manuscript). In  
55 addition, gray circles are plotted at critical SS values corresponding to diameters 20% smaller  
56 (kappa = 0.5 is assumed). This demonstrates that a decreased lower-limit diameter, and the  
57 resultant increased fractional aerosol concentration (FAC), propagate to an insignificant departure  
58 of the perturbed data points (gray circles) from the FAC relationship in Fig. 8. Certainly, the  
59 perturbed points remain within the uncertainties described in Section 4.4. This explains why we  
60 did not factor in a 20% particle-size overestimate into our analysis of uncertainty in Fig. 8.

61



62 Line 136: what height was the inlet? (this is specified only later on line 175, as 2 m) It seems to me  
63 that the aerosol inlet was much lower than is typically done for aerosol sampling campaigns (e.g.,  
64 THD has an aerosol inlet at 10m). What is the impact on the data?

65 Our main concern was keeping rain out of the Arauco inlet. We accomplished this by  
66 sampling below an eave on the west side of the residence at the Arauco Site (L136). In the  
67 revision, we modified the sentence starting on L174:

68 “An important distinction between the sampling at THD and Arauco is the above ground level  
69 (a.g.l.) height of the aerosol inlets. This is 10 and 2 m a.g.l. at THD and Arauco, respectively. We  
70 cannot state with any certainty if the lower-height sampling at Arauco made those measurements  
71 unrepresentative.”

72

73 Line 141: there is a lot of detail about the CPC principle of operation, yet this is a very commonly  
74 applied and simple instrument. In general I think the descriptions of instrumentation could be  
75 much briefer.

76 The two paragraphs were shortened and merged. However, relevant connections to the  
77 CPC at THD, maximum detectable concentration, and data recording were retained.

78 Here is the revised text:

79 “The CPC counts particles larger than  $D = 0.010 \mu\text{m}$  (Table 1) <sup>1</sup> up to a maximum concentration of  
80  $10,000 \text{ cm}^{-3}$ . The UHSAS measures scattering produced when aerosol particles are drawn through light  
81 emitted by a solid state laser ( $\lambda = 1.05 \mu\text{m}$ ). By reference to a calibration table (Cai et al. 2008; Cai et al.  
82 2013), the UHSAS microprocessor converts scattered light intensity to particle size and accumulates  
83 the derived sizes in a 99 channel histogram. Channel widths are logarithmically uniform ( $\Delta \log_{10} D =$   
84  $0.013$ ) over the instrument’s full range ( $0.055 < D < 1.0 \mu\text{m}$ ). UHSAS concentrations were recorded  
85 every 10 seconds and CPC concentrations were recorded once per second (Table 1).”

---

<sup>1</sup> The CPC minimum detectable diameters we report are in fact diameters that a CPC detects particles with efficiency = 50%. The CPC detection efficiency is a steep function of particle diameter (Weidensholer et al. 1997).

86 Line 161: the presence of the paper mill immediately render this as a non-pristine site. Later,  
87 on lines 476, the prevalence of wood burning is mentioned. Even with onshore winds, complex  
88 coastal flows will likely result in influences from these aerosol sources. Probably it needs to be  
89 stated upfront that this site is not representative of a “clean marine” location even when data are  
90 segregated by sector.

91 This is stated, after relevant analysis, in two places in the original manuscript: 1) L279 to  
92 L282, and 2) L307 to L311. We feel this is sufficient. Also, please see our reply to your General  
93 Comment.

94 Line 182: there is no mention of topography in the description of the site and surrounding  
95 area. This seems critical to understanding how the site is affected by transport.

96 The topography is provided in Fig. 1. Also, we assert that further analysis of satellite  
97 retrievals are needed to address this outstanding issue. Please see Sect. 5 where we discuss  
98 satellite-based cloud droplet concentration retrievals in Bennartz (2007).

99 Line 191: Just a comment: in the end there are only a few days (five days?) of data with  
100 onshore flow + UHSAS data that can be used to characterize the “marine” sector.

101 As we state on L191 to L192, there are 20 onshore trajectories that overlap with the availability  
102 of UHSAS measurements. Table 3, which is discussed later in the manuscript, has the dates and  
103 times of the onshore trajectories. These occurred on seven different days in June, 2015.  
104 Please note that the arrival times are static: 00, 06, 12, and 18 UTC.

105

106 Line 231-233: I don't think these equations are needed in the text – perhaps in the  
107 supplement if you think they are necessary, but they are pretty standard.

108 Yes they are standard, however, our analysis and presentation relies on these  
109 moments (zeroth, second, and third), and our CCN parameterization relies on an integral  
110 similar to Eq. 2. We prefer to leave these definitions.

111 Line 265: the T-test is a fairly standard statistical test and doesn't need a lot of description.

112 Apparently, there are a few tests in the category of "t-test". We prefer this one, and document  
113 by citing Havlicek and Crain (1988).

114

115 Line 434: internal mixing is probably not a good assumption as claimed, since many  
116 observations have shown that organics content of marine aerosol increases with decreasing  
117 size. However, it is hard to justify another assumption here, and perhaps the best way to  
118 address is to discuss some prior observations and add estimates of uncertainty?

119 Given that our parameterizations are aimed at multi-dimensional models of aerosol  
120 and cloud and multi-dimensional models of aerosol, cloud, and precipitation, where the  
121 mixing state in the activation scheme is nearly always “internal”, we do not see merit in  
122 exploring this issue. Further, we note that aerosol dynamics calculations confirm this  
123 assumption provided coagulation (of aerosol particles) and condensation (of trace gas onto  
124 aerosol particles) has gone on for 24 hours (Fierce et al. 2017; their Figure 2). The action of  
125 coalescence scavenging (Wood et al. 2006), occurring within clouds, is ignored in the  
126 calculations of Fierce et al. (2017), and would further shorten the time needed for the  
127 internal mixing assumption to be valid. Please note, we cite Fierce et al. (2017) in this  
128 paragraph of the manuscript.

129 Fierce, L., N. Riemer, and T.C. Bond, Toward Reduced Representation of Mixing State  
130 for Simulating Aerosol Effects on Climate. Bull. Amer. Meteor. Soc., 98, 971–980,  
131 <https://doi.org/10.1175/BAMS-D-16-0028.1>, 2017

132 Wood, R. ( 2006), Rate of loss of cloud droplets by coalescence in warm clouds, J.  
133 Geophys. Res., 111, D21205, doi:10.1029/2006JD007553.

134

135 CCN parameterization: why aren't the size distributions used more directly, and why fit with  
136 the exponential relationship? The latter is clearly not physical despite its long history of use  
137 on the community, although for marine stratus that do not reach high supersaturations, it is  
138 reasonable within the expected supersaturation bounds.

139 Size distributions are used in a manner that is direct. This is explained in the revised  
140 Section 4.4. Our explanation is enhanced by addition of Eq. 5 (revision).

141 What we develop is a power-function relationship between a CCN activation spectrum  
142 and supersaturation:  $N(SS) = N_{CPC} \cdot FAC(SS) = N_{CPC} \cdot C \cdot SS^k$ . As is the case for all power functions  
143 relating cumulative CCN concentration ( $N(SS)$ ) and supersaturation ( $SS$ ), cloud droplet  
144 concentration can be calculated with the activation spectrum parameters ( $C$  and  $k$ ) and with  
145 measured (or assumed) updraft velocity (e.g., Johnson 1981). Thus, an analytical link between  
146 CCN, cloud updraft, and cloud microphysics is established. Caveats associated with this  
147 approach, and why such a calculation of droplet concentration can differ somewhat from a  
148 calculation based on a numerical parcel model, are discussed in Johnson (1981).

149 Johnson, D.B., 1981: Analytical Solutions for Cloud-Drop Concentration. *J. Atmos. Sci.*,  
150 38, 215–218, [https://doi.org/10.1175/1520-0469\(1981\)038<0215:ASFDCD>2.0.CO;2](https://doi.org/10.1175/1520-0469(1981)038<0215:ASFDCD>2.0.CO;2)

151



152 What about comparing with other published spectra for coastal aerosol?

153 As far as we can tell, no published CCN activation spectra are available for the Central Chilean  
154 Pacific coast (e.g., Schmale et al. 2018). Our group has published *summertime* measurements of CCN  
155 spectra (Snider et al. 2017; their Table 2). These were acquired over the subtropical Southeast Pacific,  
156 within the summertime marine boundary layer (Snider et al. 2017; Figure 1). A comparison is shown  
157 below. Since this is an open response, we have elected to show the comparison here, but not as an  
158 addition to the manuscript. First we compare our parameterized fractional aerosol concentration (*FAC*)  
159 function to the analysis in Andreae (2009), and then we compare CCN activation spectra.

160 Fig. a (see below) reproduces the parameterized *FAC* curve presented in the manuscript (Fig. 8).  
161 As we discussed in the manuscript, this was derived using size distribution and CPC measurements  
162 (please see Eq. 5 in the revised manuscript), and using the kappa-Köhler formula of Petters and  
163 Kreidenweis (2007, their Eq. (6)). The value  $\kappa = 0.5$  is assumed for the curve we show in Fig. a. A data  
164 point derived using values in Table 2 of Andreae (2009) is also presented. Different from our approach,  
165 the measurements Andreae (2009) analyzed are from a set of CCN( $SS=0.4\%$ ) and CPC measurements.  
166 Those measurements were acquired at a variety of locations. The locations are classified as Clean  
167 Marine, Clean Continental, Polluted Marine, and Polluted Continental (Andreae 2009). The averaged  
168  $N(SS=0.4\%) / N_{CPC}$  ratio for these conditions is 0.36 (Andreae 2009; their table 2). At the large *SS* end of  
169 our parameterization (Fig. a), we see reasonable agreement between with Andreae (2009).

170 Two activation spectra – derived as  $N_{CPC} \cdot FAC(SS) = N_{CPC} \cdot C \cdot SS^k$  (Section 4.4) - are shown in Fig.  
171 b (see below). These go with upper and lower quartile values of the  $N_{CPC}$  ensemble described in the  
172 Supplementary Material (manuscript). Also presented is the averaged CCN activation spectrum based  
173 on the 36 spectra from Table 2 of Snider et al. (2017).

174 At  $SS = 0.3\%$  there is consistency between the Southern Hemisphere (SH) averaged  
175 summertime spectrum (Snider et al. 2017) and SH wintertime spectrum, provided the latter is  
176 compared using the lower-quartile- $N_{CPC}$  value (see previous paragraph). However, these averaged  
177 spectra have different slopes and they therefore diverge at  $SS < 0.3\%$ . A smaller slope in the  
178 summertime setting could be due to a less prominent Aitken mode (summertime), compared to a  
179 more prominent Aitken mode (wintertime).

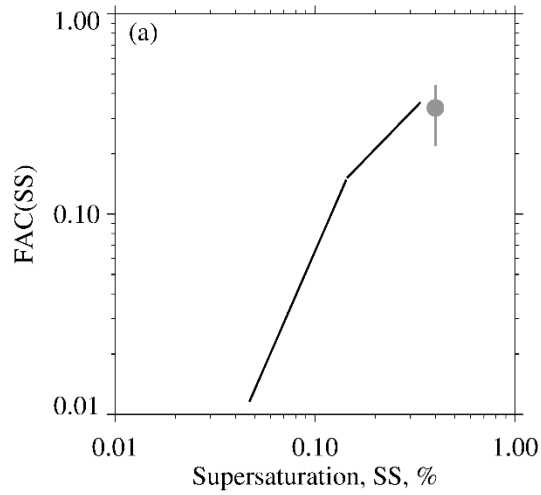
180           Although this comparison is limited, we do not see a significant discrepancy between the FAC  
181 parameterization we developed, and the approach of Andreae (2009) (Fig. a). Some discrepancy is  
182 apparent between the CCN activation spectra we derive, for relatively clean wintertime conditions,  
183 with  $N_{CPC} = 789 \text{ cm}^{-3}$ , and the averaged CCN spectrum in marine conditions over the Southeast Pacific,  
184 albeit during summer and at lower latitude. This discrepancy increases with decreasing SS. More  
185 comparison data is needed to fully validate the FAC parameterization we developed in our manuscript.

186           Andreae, M.O., Correlation between cloud condensation nuclei concentration and aerosol  
187 optical thickness in remote and polluted regions, *Atmos. Chem. Phys.*, 9, 543-556, 2009

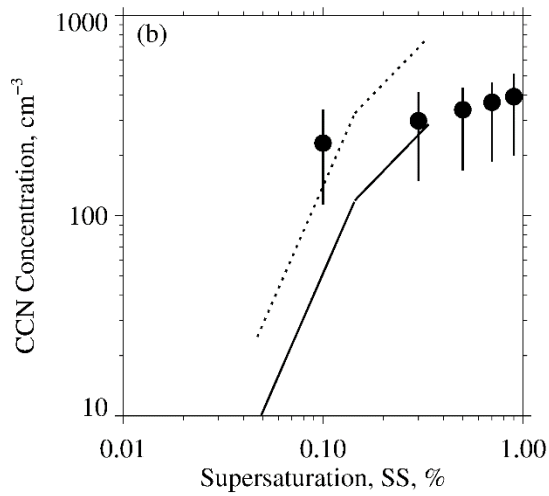
188           Petters, M. D., and S. M. Kreidenweis, A single parameter representation of hygroscopic growth  
189 and cloud condensation nucleus activity. *Atmos. Chem. Phys.*, 7, 1961–1971, 2007

190           Schmale, J., Henning, S., Decesari, S., Henzing, B., Keskinen, H., Sellegri, K., Ovadnevaite, J.,  
191 Pöhlker, M. L., Brito, J., Bougiatioti, A., Kristensson, A., Kalivitis, N., Stavroulas, I., Carbone, S., Jefferson,  
192 A., Park, M., Schlag, P., Iwamoto, Y., Aalto, P., Äijälä, M., Bukowiecki, N., Ehn, M., Frank, G., Fröhlich, R.,  
193 Frumau, A., Herrmann, E., Herrmann, H., Holzinger, R., Kos, G., Kulmala, M., Mihalopoulos, N., Nenes,  
194 A., O'Dowd, C., Petäjä, T., Picard, D., Pöhlker, C., Pöschl, U., Poulain, L., Prévôt, A. S. H., Swietlicki, E.,  
195 Andreae, M. O., Artaxo, P., Wiedensohler, A., Ogren, J., Matsuki, A., Yum, S. S., Stratmann, F.,  
196 Baltensperger, U., and Gysel, M.: Long-term cloud condensation nuclei number concentration, particle  
197 number size distribution and chemical composition measurements at regionally representative  
198 observatories, *Atmos. Chem. Phys.*, 18, 2853-2881, <https://doi.org/10.5194/acp-18-2853-2018>, 2018.

199



● Andreae (2009) Variety of Conditions (China excluded)  
 Average and Quartile Range  
 $\langle N_{\text{CPC}} \rangle = 2215 \text{ cm}^{-3}$

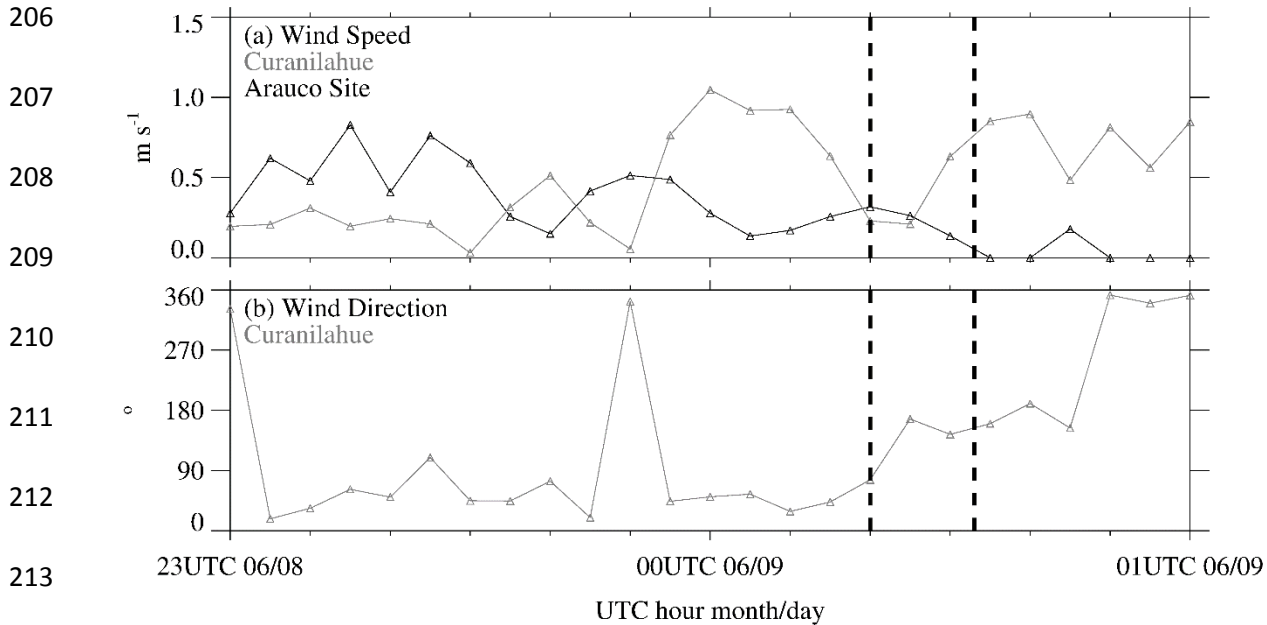


.....  $N_{\text{CPC}} = 2151 \text{ cm}^{-3}$  (Upper Quartile  $N_{\text{CPC}}$ )  
 —  $N_{\text{CPC}} = 789 \text{ cm}^{-3}$  (Lower Quartile  $N_{\text{CPC}}$ )  
 ● Snider et al. (2017) Summer Marine  
 Average and Quartile Range  
 $\langle N_{\text{CPC}} \rangle = 463 \text{ cm}^{-3}$

201

202 Figure 6: perhaps add local wind speed and direction to this figure?

203 We feel the verbal description – provided in the manuscript - is adequate. The graph is  
204 provided below, but this graph is not in the revised (or original) manuscript. In general, the  
205 effect of wind on aerosol is very difficult to interpret.



215 **Technical Corrections:**

216 Line 482: “was” should be “were”

217

218 **Corrected**

1 **Wintertime Aerosol Measurements during the Chilean Coastal Orographic**  
2 **Precipitation Experiment**

3

4 Sara Lynn Fults <sup>1</sup>

5 Adam K. Massmann <sup>2</sup>

6 Aldo Montecinos <sup>3</sup>

7 Elisabeth Andrews <sup>4,5</sup>

8 David E. Kingsmill <sup>5</sup>

9 Justin R. Minder <sup>2</sup>

10 René D. Garreaud <sup>6</sup>

11 Jefferson R. Snider <sup>1,7</sup>

12

13 <sup>1</sup> University of Wyoming, Laramie, WY

14

15 <sup>2</sup> University at Albany, Albany, NY

16

17 <sup>3</sup> Universidad de Concepción, Concepción, Chile

18

19 <sup>4</sup> NOAA ESRL Global Monitoring Division, Boulder, CO

20

21 <sup>5</sup> University of Colorado, Boulder, CO

22

23 <sup>6</sup> Universidad de Chile, Santiago, Chile

24

25 <sup>7</sup> Corresponding Author

26 **Abstract**

27           The Chilean Coastal Orographic Precipitation Experiment (CCOPE) was a three-month  
28 field campaign (June, July and August 2015) that investigated wintertime coastal rain events.  
29 Reported here are analyses of aerosol measurements made at a coastal site during CCOPE. The  
30 aerosol monitoring site was located near Arauco, Chile. Aerosol number concentrations and  
31 aerosol size distributions were acquired with a Condensation Particle Counter (CPC) and an  
32 Ultra High Sensitivity Aerosol Spectrometer (UHSAS). Arauco CPC ~~data~~ were compared to  
33 ~~values~~ measured at the NOAA observatory Trinidad Head (THD) on the North Pacific Coast of  
34 California. The winter-averaged CPC concentration at Arauco is  $2971 \text{ cm}^{-3} \pm 1802 \text{ cm}^{-3}$ ; at THD  
35 the average is  $1059 \text{ cm}^{-3} \pm 855 \text{ cm}^{-3}$ . Despite the typically more pristine Southern Pacific region,  
36 the Arauco average is larger than at THD ( $p < 0.01$ ). Aerosol size distributions~~s~~ acquired during  
37 episodes of onshore flow were analyzed with Köhler theory and used to parameterize cloud  
38 condensation nuclei activation spectra. In addition, sea salt aerosol (SSA) concentration was  
39 parameterized as a function of sea surface wind speed. It is anticipated these parameterizations  
40 will be applied in modeling of wintertime Chilean coastal precipitation.

41

Deleted: concentrations

Deleted: those

Deleted:

Deleted: measurements

46 **1 Introduction**

47 Forecast error due to incomplete understanding of atmospheric aerosols is evident in the  
48 predictions of many atmospheric models. As an example, general circulation models (GCMs) are  
49 used to forecast the Earth system's response to emissions of both aerosols and greenhouse gases.  
50 In spite of several decades of GCM development, the effect of aerosols on future climate remains  
51 uncertain (Boucher et al. 2013), particularly when compared to the greater certainty in climate  
52 forcing from anthropogenic greenhouse gases (e.g., Hansen 2009, his Fig. 10).

53 Aerosols perturb the abundance of cloud droplets and rain drops within clouds warmer  
54 than 0 °C (liquid-only clouds). Consequently, upward reflection of solar radiation by liquid-only  
55 clouds (Twomey 1974), and upward reflection attributable to cloud fractional coverage (Albrecht  
56 1989), increase with increased aerosol abundance. Commonly referred to as aerosol indirect  
57 effects on climate, these processes decrease the amount of solar energy absorbed by the Earth  
58 system, and thus oppose global warming due to greenhouse gases. Other aerosol indirect effects,  
59 for example those due to aerosols nucleating ice in mixed-phase clouds (McCoy et al., 2014),  
60 augment greenhouse gas warming.

61 Because of its lower population and lower intensity of anthropogenic aerosol emissions,  
62 the Southern Hemisphere has been explored as a region for conducting studies of aerosol indirect  
63 effects and for exploring contrasts with the Northern Hemisphere (Schwartz, 1988). This study  
64 contributes to previous investigations of Southern Hemispheric aerosols during winter (Gras,  
65 1990; Gras 1995; Yum and Hudson 2004). We emphasize the following topics: 1) The  
66 parameterized relationship between sea salt aerosol (SSA) particles (diameter > 0.5 μm) and  
67 wind speed; 2) The role as cloud condensation nuclei (CCN) of particles that are both smaller  
68 and more numerous than the above-mentioned SSA; 3) The parameterized relationship

**Deleted:** Via this interaction, both upward reflection of solar radiation by cloud cover (Albrecht 1989), and upward reflection by individual cloud elements (Twomey 1974) increase with increased aerosol abundance.

**Deleted:** Because of its lower population and lower intensity of anthropogenic aerosol emissions, the Southern Hemisphere has been explored as a region for conducting studies of aerosol indirect effects and for exploring contrasts with the Northern Hemisphere (Schwartz, 1988; Gras, 1990; Gras 1995; Yum and Hudson 2004). This study contributes to those previous wintertime investigations of Southern Hemispheric aerosols.

80 describing CCN activation spectra (Rogers and Yau, 1989; chapter 6), and 4) the potential  
81 application of the SSA and CCN parameterizations in numerical modelling of wintertime  
82 Southern Hemispheric clouds and precipitation. Motivating our investigation are modeling  
83 studies (Feingold et al. 1999), and analyses of field measurements (Gerber and Frick 2012),  
84 indicating that the reduction of rainfall due to increased CCN can be negated by SSA particles.

**Deleted:** We emphasize the following topics: 1) The parameterized relationship between sea salt aerosol (SSA) concentration and sea surface wind speed; 2) The concentration of aerosol particles that are both smaller and more numerous than the SSA, and their role as cloud condensation nuclei (CCN); 3) The parameterized relationship describing CCN activation spectra (Rogers and Yau, 1989; chapter 6), and 4) the potential application of the SSA and CCN parameterizations in numerical modelling of wintertime Southern Hemispheric clouds and precipitation. Motivating our investigation are modeling studies (Feingold et al. 1999), and analyses of field measurements (Gerber and Frick 2012), indicating that the reduction of rainfall due to increased CCN can be negated by SSA particles.

85 Measurements made with a Condensation Particle Counter (CPC), an instrument that  
86 reports the concentration of particles with diameter ( $D$ ) larger than  $\sim 0.01 \mu\text{m}$ , have formed the  
87 basis of many previous investigations of aerosol abundance (Gras 1990; Brechtel et al. 1998;  
88 Dall'Osto et al. 2009; Andreae 2009). These studies also evaluated air parcel back trajectories  
89 and demonstrated that marine source regions are characterized by distinctly smaller  
90 concentrations than continental regions. Measurements of aerosol size distributions (ASDs) can  
91 also aid understanding of the contrast between marine and continental conditions (Brechtel et al.  
92 1998; Birmili et al. 2001; Raes et al. 1997). The latter studies investigated accumulation mode  
93 particles, centered at  $\sim 0.1 \mu\text{m}$ , and particles sizing in a mode at a distinctly smaller central  
94 diameter ( $\sim 0.05 \mu\text{m}$ ). This smaller mode is commonly referred to as the Aitken mode. In marine  
95 settings, the coexistence of both modes has been attributed to in-cloud conversion of gas-phase  
96 sulfur dioxide ( $\text{SO}_2$ ) to aerosol-phase sulfate (Hoppel et al. 1994), to coalescence scavenging  
97 occurring within clouds (Hudson et al. 2015), and to new particle formation (Covert et al. 1992;  
98 Petters et al. 2006). The latter process occurs in environments with sufficiently enhanced ratios  
99 of  $\text{SO}_2$  relative to aerosol.

**Deleted:** CPC

**Deleted:** CPC concentrations

100 The present work is an analysis of CPC and ASD measurements acquired at a coastal site  
101 on the Central Chilean Pacific coast during the Southern Hemisphere winter (June, July, and  
102 August). Aerosol measurements were made during the Chilean Coastal Orographic Precipitation

**Deleted:** concentrations and

**Deleted:** s

**Deleted:** d



121 Experiment (CCOPE) of 2015. CCOPE investigated aerosol properties and coastal orographic  
122 precipitation and meteorology (Massmann et al. 2017).

123 This paper is organized into the following sections: Section 2 has descriptions of the  
124 aerosol and meteorological instruments used to make surface measurements during CCOPE, and  
125 Sect. 3 describes our analysis methods. Section 4 includes four topics: 1) Analysis of CPC  
126 measurements and comparison to Coastal North Pacific measurements, 2) development of a  
127 relationship between size-integrated aerosol concentration and size-integrated aerosol volume,  
128 and comparison to similar relationships derived for summertime stratocumulus regimes, 3)  
129 development of a parameterization of CCN activation spectra, and 4) development of a  
130 parameterization of SSA number concentration. In Sect. 5, we compare our findings to previous  
131 work, and in Sect. 6 we conclude with an outlook for how our parameterizations could be applied  
132 in modeling of wintertime Central Chilean Pacific coast clouds and precipitation.

Deleted: A

## 133 2 Measurements

### 134 2.1 Measurement Site

135 During CCOPE, a CPC (model 3010; TSI 2000a) and an Ultra High Sensitivity Aerosol  
136 Spectrometer (UHSAS) (DMT 2013) were operated at a residence (37.25° S, 73.34° W, 55 m  
137 above mean sea level (MSL)) near Arauco, Chile (population 35,000). Arauco is a coastal town  
138 on the Central Chilean Pacific coast. Our measurement site, hereafter the Arauco Site (Fig. 1),  
139 was selected because of our aim to characterize aerosols advecting onto South America from the  
140 Southeast Pacific. Related to this, our measurements were coordinated with investigations of  
141 rainfall inside the domain portrayed in Fig. 1. This study region lies in the South Pacific winter  
142 storm track and rainfall here can be strongly enhanced by the Nahuelbuta Mountains (Garreaud

144 et al. 2016; Massmann et al. 2017). During CCOPE, several rainfall events were studied using  
145 profiling radars and a precipitation disdrometer deployed at Curanilahue (Fig. 1), and a network  
146 of precipitation gauges. The Arauco Site is located on a forested hill; most of the population of  
147 Arauco lives east of the Arauco Site at an elevation less than 20 m MSL.

148 Salient characteristics of the CPC and UHSAS are provided in Table 1. These  
149 instruments were operated inside the residence at the Arauco Site. In addition, a 3-meter  
150 meteorological tower was deployed adjacent to the residence. Thermodynamic state (i.e.,  $T$ ,  $P$ ,  
151 and humidity) and horizontal wind speed and direction were measured on the tower. CPC and  
152 meteorological measurements (minus wind direction) were acquired from 29 May to 14 August  
153 (Table 1), UHSAS measurements were acquired from 29 May to 28 June (Table 1), and wind  
154 direction measurements were acquired from 19 June to 14 August.

## 155 2.2 Instrumentation

156 Here we discuss characteristics of the CPC and UHSAS, sampling of the ambient  
157 CCOPE aerosol, data acquisition of CPC and UHSAS measurements during CCOPE, and use of  
158 the recorded UHSAS histograms to calculate ASDs. Additional information about the UHSAS is  
159 provided in Appendix A. In that appendix we discuss how we validated, in a laboratory, the  
160 UHSAS's determination of test aerosol concentration and particle size. During those validation  
161 studies we intentionally dried the test aerosols to a relative humidity ( $RH$ )  $\leq 15\%$ . Consequently,  
162 the effect of aerosol-bound water on either the physical size or the refractive index of the test  
163 particles was negligible. UHSAS sizing of partially dried haze droplets ( $RH \leq 60\%$ ), sampled  
164 from the ambient atmosphere during CCOPE, and an associated particle size overestimate, is  
165 also discussed in Appendix A. In Appendix A, we estimate the particle size overestimate to be ~  
166 20 %.

167 During CCOPE, the CPC and UHSAS sampled ambient aerosol through a section of  
 168 copper tube (length = 3 m, inner diameter = 0.003 m, volumetric flow rate = 34 cm<sup>3</sup> s<sup>-1</sup>). The  
 169 inlet end of the tube (hereafter, the sample tube) was secured below an eave on the west side of  
 170 the residence at the Arauco Site. The Reynolds number (*Re*) of the flow within the sample tube  
 171 was 960 and thus well below the value (*Re* = 2300) where laminar flow changes to turbulent  
 172 flow. Particle transmission efficiencies were evaluated using Eq. (7.29) in Hinds (1999). These  
 173 are 78% for *D* = 0.01 μm particles and ≥ 99% for *D* = 0.1 μm and *D* = 1 μm particles.

174 The CPC counts particles larger than *D* = 0.012 μm (Table 1)<sup>1</sup> up to a maximum  
 175 concentration of 10,000 cm<sup>-3</sup>. The UHSAS measures scattering produced when aerosol particles  
 176 are drawn through light emitted by a solid state laser (*λ* = 1.05 μm). By reference to a calibration  
 177 table (Cai et al. 2008; Cai et al. 2013), the UHSAS microprocessor converts scattered light  
 178 intensity to particle size and accumulates the derived sizes in a 99 channel histogram. Channel  
 179 widths are logarithmically uniform ( $\Delta \log_{10} D = 0.013$ ) over the instrument's full range ( $0.055 < D$   
 180 < 1.0 μm). UHSAS data were recorded every 10 seconds and CPC data were recorded once per  
 181 second (Table 1).

Formatted: Font: Italic

Formatted: Superscript

Formatted: Subscript

Formatted: Font: Italic

Formatted: Font: Italic

**Deleted:** The CPC counts particles larger than *D* = 0.010 μm (Table 1)<sup>2</sup> by detecting scattering produced when aerosol particles are drawn through light emitted by a solid state laser (*λ* = 0.78 μm). Prior to detection, the particle diameter is increased by at least a factor of 10 via alcohol condensation. The aerosol sample flowrate in the CPC was 16 cm<sup>3</sup> s<sup>-1</sup>. The CPC can detect a maximum concentration of 10,000 cm<sup>-3</sup>. During CCOPE, CPC concentrations were recorded once per second and once every 10 seconds (Table 1). The UHSAS measures scattering produced when aerosol particles are drawn through light emitted by a solid state laser (*λ* = 1.05 μm). By reference to a calibration table (Cai et al. 2008; Cai et al. 2013), the UHSAS microprocessor converts scattered light intensity to particle size and accumulates the derived sizes in a 99 channel histogram. Channel widths are logarithmically uniform ( $\Delta \log_{10} D = 0.013$ ) over the instrument's full range ( $0.055 < D < 1.0 \mu\text{m}$ ). During CCOPE, the aerosol sample flow in the UHSAS was controlled at 0.34 cm<sup>3</sup> s<sup>-1</sup>.

182 Eq. (1) was used to calculate the ASD.

$$183 \left( \frac{dN}{d \log_{10} D} \right)_i = \frac{\Delta n_i}{\dot{V} \cdot \Delta t \cdot \Delta \log_{10} D} \quad (1)$$

184 Here  $\Delta n_i$  is the “i th” component of the count histogram and  $\dot{V}$  is the aerosol flowrate. During  
 185 CCOPE, the UHSAS aerosol flow rate and the particle count histogram were recorded once  
 186 every ten seconds (Table 1), and hence, the sample interval ( $\Delta t$  in Eq. (1)) is 10 s.

<sup>1</sup> The CPC minimum detectable diameters we report are in fact diameters that a CPC detects particles with efficiency = 50 %. The CPC detection efficiency is a steep function of particle diameter (Wiedensohler et al. 1997).

204 **3 Analysis**

205 **3.1 Air Mass Classification and Air Parcel Trajectories**

206 Locations close to the Arauco Site are shown in Fig. 1. A significant pollution source in  
207 the region is the Arauco paper mill which releases 600 ton/yr of SO<sub>2</sub> (Arauco Woodpulp 2010).  
208 When winds had an easterly component, the paper mill may have affected air quality at the  
209 Arauco Site. Other pollution sources are ~~Concepción (population 950,000), Coronel (population~~  
210 ~~110,000), Curanilahue (population 32,000), Lebu (population 24,000), and Cañete (population~~  
211 ~~32,000).~~ In addition, many residences in the region, including the residence where we operated  
212 the CPC and UHSAS, burn wood for residential heating.

**Deleted:** Curanilahue (population 32,000) and

**Deleted:** ; this includes several municipalities adjacent to Concepción

**Deleted:** .

213 In a subsequent section, we compare CPC ~~data~~ from the Arauco Site to values measured  
214 at NOAA's Trinidad Head (THD) observatory in Northern California (41.05° N, 124.2° W, 107  
215 m MSL). The THD dataset includes contamination from local sources (e.g., campfires lit by day  
216 visitors at the Trinidad State Beach Picnic Ground). Additionally, Mckinleyville, CA (population  
217 15,000) and Arcata, CA (population 18,000) are the two coastal population centers reasonably  
218 close to THD. Both are southeast of the THD, at distances between 15 and 25 km. Northern  
219 California's large population centers (San Francisco Bay Area and Sacramento) are ~ 300 km  
220 southeast of the THD. ~~An important distinction between the sampling at THD and Arauco is the~~  
221 ~~above ground level (a.g.l.) height of the aerosol inlets. This is 10 and 2 m a.g.l. at THD and~~  
222 ~~Arauco, respectively. We cannot state with any certainty if the lower-height sampling at Arauco~~  
223 ~~made those measurements unrepresentative.~~

**Deleted:** concentrations

**Deleted:** An important distinction between the sampling at THD and Arauco is the above ground level (a.g.l.) height of the aerosol inlets. This is 10 and 2 m a.g.l. at THD and Arauco, respectively.

224 Wind measurements made at the Arauco Site (Sect. 2.1) and the THD were used to  
225 conditionally sample the CPC measurements. At Arauco, wind directions from 180° to 330°  
226 were chosen as the clean sector. At THD, the clean sector was chosen from 210° to 360°. The

235 clean sectors at Arauco and THD are shown in Fig. 2. Three factors entered into our selection of  
236 the clean sectors: 1) Inclusion of winds from either true south (Arauco Site) or true north (THD),  
237 2) the same range of angles (150°) at both sites, and 3) exclusion of wind from the directions of  
238 regional population centers.

239         Additionally, we used HYSPLIT back trajectories (NOAA 2016) to conditionally sample  
240 Arauco Site aerosol measurements associated with onshore-moving air. The back trajectories  
241 were initialized at 00, 06, 12, and 18 UTC. In addition to these static arrival times, trajectories  
242 were calculated with the coordinates of the Arauco Site <sup>3</sup> and with wind fields from the Global  
243 Data Assimilation System. The spatial resolution of the wind data is 0.5°. Position along a  
244 trajectory was evaluated hourly. Trajectories that were over the ocean continuously for three  
245 days before landfall, and had a direction within the clean sector one hour before arriving at  
246 Arauco, were classified as “onshore” trajectories. There are 20 onshore trajectories that overlap  
247 with the availability of CCOPE UHSAS measurements.

248         In subsequent sections, a set of 20 two-hour data segments, centered on the onshore  
249 trajectory arrival times, are further analyzed. Appendix B describes the numerical filter we used  
250 to derive the aerosol properties analyzed in Sect. 4.2, 4.3, 4.4, and 4.5. The filter attenuates  
251 aerosol property variability occurring on time scales shorter than 100 s. We developed the filter  
252 to remove narrow “spikes” in the concentration sequences (CPC and UHSAS) which seem to  
253 have originated from local sources of aerosol pollution. The Supplementary Material has plots of  
254 filtered aerosol properties corresponding to each of the 20 two-hour segments. Four of these  
255 were impacted aerosol variability at scales larger than 100 s. In general, these features were not

---

<sup>3</sup> Trajectory starting altitude was set at 60 m MSL (5 m above the Arauco site)

256 attenuated by the numerical filter. In these instances we discarded (subjectively) portions of the  
257 two-hour segment and retained a subset for the analyses conducted in Sect. 4.3, 4.4 and 4.5.

258 Trajectory altitude is important for determining the presence of SSA particles. Onshore  
259 trajectories originating from relatively close to the sea surface, and thus classified as onshore  
260 “sea surface” trajectories, were required to have pressures  $> 980$  hPa over their three-day  
261 advection to the Arauco Site. Eighteen of the 20 onshore trajectories were also sea surface  
262 trajectories. An example of a sea surface trajectory is shown in Figs. 3a - b. The sea surface wind  
263 speed ( $U$ ), analyzed in Sect. 4.5, is the average of the six hourly trajectory speeds in the six-hour  
264 window ending six hours before the trajectory arrived at the Arauco site. The averaging interval  
265 is shown in Fig. 3b. Two onshore trajectories, classified as “aloft”, had pressures substantially  
266 smaller than 980 hPa over their three-day advection to the Arauco Site.

### 267 3.2 Sea Salt Aerosol

268 Correlated values of SSA concentration and sea surface wind speed are reported in many  
269 publications. In a review of the topic, Lewis and Schwartz (2004; hereafter LS04) used a  
270 particle’s deliquesced wet size, evaluated at 80% relative humidity, to group SSA particles into  
271 three size classes. In field studies conducted at a coastal site, Clarke et al. (2003) demonstrated  
272 that particles sizing in the middle of LS04’s small particle size class - those with a dry diameter  
273 larger than  $0.5 \mu\text{m}$  or a  $RH = 80\%$  wet diameter larger than  $1 \mu\text{m}$  – had a composition that was  
274 dominated by sea salt (NaCl).

275 By restricting our focus to segments of the CCOPE data associated with sea surface  
276 trajectories (Sect. 3.1), we will analyze UHSAS measurements of particles with  $D > 0.5 \mu\text{m}$   
277 ( $N_{>0.5}$ ) and will assume that this subset of the ASD corresponds to SSA particles. This lower-  
278 limit size is a factor of two smaller than the  $RH = 80\%$  diameter corresponding to the middle of

Deleted: -derived concentrations

280 LS04's small SSA class. This is because we assumed that particle size decreased as the aerosol  
281 stream warmed from its ambient temperature to the temperature of the UHSAS measurement.  
282 Support for this assumption is provided in Appendix A.

### 283 3.3 Moments of the Aerosol Size Distribution

284 In our analysis, we calculated three moments of the UHSAS-measured ASDs. These are  
285 the aerosol concentration ( $N_{UHSAS}$ ), aerosol surface area ( $S_{UHSAS}$ ), and aerosol volume ( $V_{UHSAS}$ ).  
286 We symbolize these moments as integrals (Eq. (2) – (4)).

$$287 \quad N_{UHSAS} = \int (dN/d\log_{10}D) \cdot d\log_{10}D \quad (2)$$

$$288 \quad S_{UHSAS} = \pi \int D^2 (dN/d\log_{10}D) \cdot d\log_{10}D \quad (3)$$

$$289 \quad V_{UHSAS} = (\pi/6) \int D^3 (dN/d\log_{10}D) \cdot d\log_{10}D \quad (4)$$

290 In these formulae the group  $(dN/d\log_{10}D) \cdot d\log_{10}D$  represents the concentration of aerosol  
291 particles with diameter between  $\log_{10}D$  and  $\log_{10}D + d\log_{10}D$ . Hence, when plotted versus the  
292 logarithm of particle diameter, the area under the  $dN/d\log_{10}D$  curve is proportional to the size-  
293 integrated concentration. This is demonstrated in Figs. 4a – b where the size-integrated  
294 concentration is  $\sim 300 \text{ cm}^{-3}$  in onshore-moving air (Fig. 4a), and the concentration is  
295 approximately four times larger ( $\sim 1100 \text{ cm}^{-3}$ ) in air thought to be contaminated by continental  
296 sources (Fig. 4b). Also apparent is the right-tail of an Aitken mode, at  $\sim 0.06 \mu\text{m}$  in Fig. 4a  
297 (onshore-moving air), the absence of an Aitken mode in Fig. 4b (continental air), at least at  
298 diameters detectable by the UHSAS ( $D > 0.055 \mu\text{m}$ ; Table 1), and the presence of an  
299 accumulation mode at  $\sim 0.1 \mu\text{m}$  in both airmasses (Figs. 4a – b). Two aspects of these results, i.e.  
300 the absence of an Aitken mode plus the dominance of an accumulation mode, in polluted coastal  
301 air, is consistent with ASDs reported in Raes et al. (1997) and in Dall'Osto et al. (2009).

Deleted: ( $N_{UHSAS}$ )

303 4 Results

304 4.1 Comparison of CPC ~~data from the Arauco Site and the THD~~

305 In this section, ~~CPC-measured concentrations from the Arauco Site and from~~ NOAA's  
306 THD observatory ~~are compared~~. At THD, ~~CPC measurements were made~~, using a TSI 3760  
307 condensation particle counter. The minimum particle diameter detected by the TSI 3760 ( $D =$   
308  $0.015 \mu\text{m}$ ; ~~Wiedensohler et al. 1997~~) is slightly larger than that in the TSI 3010 ( $D = 0.012 \mu\text{m}$ ;  
309 Table 1). We ignored this distinction.

310 The THD dataset spans the years 2002 to 2014. Because CCOPE was a wintertime field  
311 study, only December, January, and February THD data are used in the comparison. There are  
312 24,346 data points (hourly averaged) from THD and 5,541 classify as clean sector. In  
313 comparison, there are 745 data points from the Arauco Site (hourly averaged) and 194 classify as  
314 clean sector. For both sites, we required a clean sector wind speed  $> 1.5 \text{ m s}^{-1}$  in addition to the  
315 clean sector directional criteria (Fig. 2). Because the numerical filter (Sect. 3.1) requires 1 Hz  
316 CPC measurements, and since 1 Hz measurements are unavailable in the THD data archive, the  
317 filter was not applied to either of the data sets analyzed in this section.

318 In the following paragraph we compare ~~hourly-averaged CPC-measured concentrations~~  
319 ~~from the Arauco Site and THD~~. Because the number of data points in these data sets is different,  
320 a particular statistical comparison methodology was applied. The approach followed here  
321 compares the Arauco and THD average concentrations by applying the Student's t-distribution  
322 method (t-test) explained in Havlicek and Crain (1988; their Eq. (10.6) and (10.7)). The  
323 statistical hypotheses are: A) Null hypothesis: averages are equal, and B) Alternate hypothesis:  
324 ~~averages are different~~. We also applied the non-parametric Wilcoxon Rank-Sum Test (`rs_test`;  
325 Interactive Data Language, Harris Geospatial Solutions, Inc.). Statistical inference that we derive

Deleted: Concentrations at

Deleted: Arauco site

Deleted: concentrations are compared to concentrations measured at

Deleted: concentrations were measured

Deleted: 1

Deleted: TSI 1996

Deleted: 0

Deleted: hourly averages of CPC measurements

Deleted: the



336 based on the Wilcoxon Rank-Sum Test (not shown) is consistent with what we describe below  
337 using the t-test.

338 Two aspects of the Arauco/THD comparison are presented here; more detail is available

339 in Fults (2016). First, clean sector measurements are compared. The mean  $N_{CPC}$  at Arauco is  
340  $2759 \text{ cm}^{-3}$  (standard deviation  $\sigma = 1827 \text{ cm}^{-3}$ ). The mean and  $\sigma$  at THD are  $858 \pm 729 \text{ cm}^{-3}$ . Fig. 5

Deleted: concentrations

341 shows the Arauco and THD  $N_{CPC}$  probability distribution functions. Of note is the larger mode  
342 concentration and broader distribution at Arauco. Based on our t-test comparison, the Arauco

343 average is larger than the THD average ( $p < 0.01$ ). Second, Arauco and THD concentrations are  
344 compared without regard to wind direction. The average at the Arauco Site is  $2971 \text{ cm}^{-3} \pm 1802$

Deleted: concentrations

345 while at THD the average is  $1059 \text{ cm}^{-3} \pm 855 \text{ cm}^{-3}$ . These averages are also statistically different  
346 ( $p < 0.01$ ), and again, the Arauco average is larger than that at THD. Based on averages

347 presented in this section, and information provided in Table 2, two summary statements are

348 warranted: 1) During wintertime, the THD classifies as a moderately-polluted marine site,

349 and the Arauco Site classifies between moderately-polluted marine and heavily-polluted

350 marine. 2) These sites are not representative of conditions well removed from anthropogenic

## 352 4.2 Continental Contamination

353 In this section we probe why aerosol properties varied strongly during four of the 20  
354 onshore trajectories. Among these, the example presented in Figs. 6a – c exhibits the largest  
355 degree of CPC and UHSAS variability. During this two-hour data segment, centered on 00 UTC

356 June 9 (9 pm local time), winds were light at Arauco and Curanilahue ( $\leq 1 \text{ m s}^{-1}$ ) and the wind

Deleted: < 2

357 direction was variable at Curanilahue (Arauco Site wind direction measurements are only

358 available after 19 June 2015; Sect. 2.1).

366 Over the ocean, 12 to 6 hours prior to 00 UTC June 9, the HYSPLIT wind speed was 8.3  
367 m s<sup>-1</sup> and the HYSPLIT direction was westerly (Fig. 3a). In terms of UHSAS measurements  
368 (Figs. 6a – c), an obvious feature is the variability in the sequences of  $N_{UHSAS}$ ,  $V_{UHSAS}$ , and  $S_{UHSAS}$ .  
369 The  $S_{UHSAS}$  is largest during an enhancement at ~ 00:37 UTC. The question arises: Can winds  
370 over the ocean and the resultant SSA production cause this variability, or must continental  
371 aerosol sources be evoked to explain this? This was addressed by calculating aerosol surface  
372 areas as a function of wind speeds that bracket the HYSPLIT-derived wind speed (8.3 m s<sup>-1</sup>). The  
373 basis for this calculation is the *S-on-U* parameterization described in LS04 (their Fig. 22). The  
374 calculation indicates that  $S$  can range between 6 μm<sup>2</sup> cm<sup>-3</sup> ( $U = 6.3$  m s<sup>-1</sup>) and 15 μm<sup>2</sup> cm<sup>-3</sup> ( $U =$   
375 10.3 m s<sup>-1</sup>). Since the upper-limit of the predicted variation is small compared to  $S_{UHSAS}$  at ~  
376 00:37 UTC (Fig. 6c), and at other times in Fig. 6c, and because the wind speed variation applied  
377 in the calculation is an order of magnitude larger than the variation in the HYSPLIT-derived  
378 wind speed ( $\pm 0.1$  m s<sup>-1</sup>), it is concluded that the aerosol enhancements seen in Figs. 6a – c are  
379 not due to a wind speed increase over the ocean. Rather, we surmise that aerosols emitted by  
380 continental Chilean sources were sampled during portions of the segment in Fig. 6. Vertical  
381 dashed lines indicate the subset of the two-hour segment we picked (subjectively) as being  
382 representative of onshore-moving air that was not affected, or only moderately affected, by  
383 emissions from continental Chilean sources. However, we do not expect our conditional  
384 sampling (based on HYSPLIT) and subjective picking (e.g., Fig. 6) to select aerosol properties  
385 representative of pristine marine air. Rather, we view these strategies as way to isolate aerosol  
386 properties associated with onshore-moving air that was less affected by continental sources  
387 compared to the other portions of the CCOPE data set.

Deleted: b

389 Portions of three other two-hour segments were also discriminated into a period of  
390 onshore-moving air that was less affected by continental aerosols compared to an adjacent  
391 portion (or portions) of the two-hour data segment. This is shown in the Supplementary Material.  
392 Only measurements seen plotted between the vertical dashed lines in the Supplementary Material  
393 are analyzed in Sect. 4.3, 4.4, and 4.5.

### 394 4.3 Using $N/V$ ratios to Parameterize Cloud Droplet Concentration

395 In this section we analyze two ASD moments (Sect. 3.3). These are symbolized  $N_{UHSAS}$   
396 and  $V_{UHSAS}$ , respectively. The ratio of  $N_{UHSAS}$  (aerosol concentration) and  $V_{UHSAS}$  (aerosol volume)  
397 – generically the  $N/V$  ratio – is of interest for several reasons. First, for both operational and  
398 theoretical reasons the  $N/V$  ratio is evaluated for particle diameters larger than  $\sim 0.1 \mu\text{m}$  (VD00;  
399 Hegg and Kaufman 1998, hereafter HK98), and importantly, the model developed to evaluate  
400 aerosol exchange between an overlying free troposphere (FT) and the marine boundary layer  
401 (MBL) successfully predicts the  $N/V$  ratio in the MBL (VD00). Second, a value of the ratio can  
402 be derived by fitting measurements of  $N$  and  $V$  (HK98). Third, aerosol mass loading, and thus an  
403 aerosol volume corresponding to an assumed particle density<sup>4</sup>, are relatively easy to evaluate. A  
404 method routinely used to evaluate aerosol mass loading involves pulling aerosol-laden air  
405 through a filter and evaluating the accumulated mass gravimetrically. Fourth, the product of an  
406  $N/V$  ratio and an ambient aerosol volume (aerosol mass) has been proposed as a scheme for  
407 estimating cloud droplet concentration in marine stratocumulus clouds (HK98 and VD00).

408 HK98 used a passive cavity aerosol spectrometer probe (PCASP) to evaluate  $N$ ,  $V$  and the  
409  $N/V$  ratio. Since the UHSAS counts down to a smaller diameter ( $0.055 \mu\text{m}$ ) than the PCASP

Deleted: s

Formatted: Font color: Text 1

Deleted: the

Formatted: Font color: Text 1

Deleted: defined by Eq. (2) and (4)

Formatted: Font color: Text 1

Formatted: Font color: Text 1

Formatted: Font: Italic

Formatted: Font color: Text 1

Deleted: models that evaluate exchange between a marine boundary layer (MBL) and an overlying free troposphere (FT) successfully predict the  $N/V$  ratio in the MBL (van Dingenen et al., 2000; hereafter VD00). Second, a value of the ratio can be derived by fitting measurements of  $N$  and  $V$  (Hegg and Kaufman 1998, hereafter HK98). Third, aerosol mass loading, and thus an aerosol volume corresponding to an assumed particle density

Formatted: Font color: Text 1

Deleted: are relatively easy to evaluate. A method routinely used to evaluate aerosol mass involves pulling aerosol-laden air through a filter and evaluating the accumulated mass gravimetrically. Fourth, the product of an  $N/V$  ratio and an ambient aerosol volume has been proposed for estimating cloud droplet concentrations in marine stratocumulus clouds (HK98 and VD00).

<sup>4</sup> In the case of ambient particles containing hygroscopic materials, density values range between  $1.5$  and  $1.8 \text{ g cm}^{-3}$  (McMurry et al. 2002)

426 (0.12  $\mu\text{m}$ ), it is expected that the  $N/V$  ratios we derive using the UHSAS will be larger than those  
427 in HK98. The main reason for this is that decreasing the lower-limit diameter increases  $N$  more  
428 than  $V$  (VD00).

429 As in HK98, linear least-squares regression analysis with an equation of the form  $Y = a \cdot X$   
430 was used to derive  $N/V$  ratios. Values of  $N_{UHSAS}$  and  $V_{UHSAS}$  entered into the regressions were  
431 derived with the lower-limit diameter set at 0.055  $\mu\text{m}$  (Table 3) and 0.12  $\mu\text{m}$  (Table 4). The latter  
432 allows comparison to  $N/V$  ratios in HK98. Tables 3 and 4 show the ratios and the fact that all of  
433 the Pearson correlation coefficients ( $r$ ) are positive. With the exception of trajectories arriving at  
434 12 UTC June 5 and 06 UTC June 8 (Table 3), and at 00 UTC June 9 (Table 4), all of the  $N/V$   
435 correlations are statistically significant at  $p < 0.01$ .

436 As expected, the average  $N/V$  ratio in the fifth column of Table 3 ( $417 \pm 297 \mu\text{m}^{-3}$ ) is  
437 larger than that in HK98 ( $223 \pm 76 \mu\text{m}^{-3}$ ). These averages are different at  $p = 0.01$ . Table 4 has  
438 results based on the larger lower-limit diameter (0.12  $\mu\text{m}$ ). In that comparison, the Arauco  $N/V$   
439 ratio ( $159 \pm 100 \mu\text{m}^{-3}$ ) does not differ significantly from HK98's (i.e.,  $p > 0.01$ ).

440 Application of the  $N/V$  ratio to aerosol-cloud-precipitation modelling requires knowledge  
441 of the aerosol volume, or alternatively, knowledge of the aerosol mass loading and the aerosol  
442 particle density. The aerosol volume is then multiplied by an average  $N/V$  ratio (e.g., the average  
443 at the bottom of the fifth column of Table 4), and their product is taken to be the modelled cloud  
444 droplet concentration (HK98 and VD00). This is straight forward, at least from the perspective of  
445 incorporating an aerosol-induced cloud feedback into a simulation, but it suffers from requiring  
446 additional information about the aerosol (aerosol volume). Because the UHSAS was unavailable  
447 for much of CCOPE (Table 1), aerosol volume is also unavailable. Another drawback is the

448 implicit assumption that only aerosol particles larger than the lower-limit diameter (e.g., 0.12 μm  
449 in Table 4) form cloud droplets.

#### 450 4.4 Using Size Distribution and N<sub>CPC</sub> to Parameterize CCN Activation Spectra

451 Andreae (2009) analyzed a set of aerosol concentration measurements obtained from  
452 collocated CPC and CCN instruments. Andreae's CPC measurements represent the concentration  
453 of particles *no smaller than* a particular diameter (~ 0.01 μm; Sect. 2.2), and his CCN  
454 measurements represent the concentration of particles that activate cloud droplets at a water  
455 vapor supersaturation (*SS*) *no larger than* a particular value (Rogers and Yau, 1989; chapter 6).  
456 The latter is *SS* = 0.4 % in Andreae (2009).

457 Similar to the relationship between CCN concentration at *SS* = 0.4 % and CPC  
458 concentration (Andreae, 2009; his Fig. 2), we now describe how CPC and UHSAS data from  
459 CCOPE can be used to develop a function that describes CCN activation spectra. In the  
460 parameterization we develop, the independent variable is a CPC-measured aerosol concentration.  
461 While only estimates, the activation spectra we obtain represent an important step toward  
462 evaluating how CCN affected cloud and precipitation during CCOPE. We envision this  
463 assessment will be advanced when our activation spectra are used to initialize numerical models.

464 Our first step is to select a particle diameter, apply this as a lower-limit diameter in an  
465 integration of the UHSAS size distribution, and divide the integral by the coincident CPC-  
466 measured concentration. The resultant is referred to as the fractional aerosol concentration  
467 (FAC).

$$468 \quad FAC(D) = \frac{1}{N_{CPC}} \cdot \int_D^{1\mu m} (dN / d \log_{10} D) \cdot d \log_{10} D \quad (5)$$

469 Figs. 7a - b have graphical representations of FAC(D=0.055 μm) and FAC(D=0.120 μm)

Deleted: ASD and N<sub>CPC</sub> Measurements

Deleted: Table 1

Deleted: s

Deleted: s

Deleted: concentrations

Deleted: s

Deleted: our development

Deleted: that

Deleted: Eq. (2)

Deleted: resultant size-integrated UHSAS

Deleted: concentration

Formatted: Font: Italic

Formatted: Font: Italic

Deleted: Two examples of this are presented in Figs. 7a - b where we define the UHSAS-to-CPC concentration ratio as a *fractional aerosol concentration (FAC)*.

Formatted: j\_para\_no\_indent, Indent: First line: 0.5"

Field Code Changed

Formatted: j\_para\_no\_indent

Deleted: We symbolize these

Deleted: as

Deleted: (Fig. 7a)

Deleted: as

Deleted: ) (Fig. 7b). As is illustrated, a *FAC* can be interpreted as the fraction of the aerosol population *no smaller than* the lower-limit diameter at the left-edge of the gray shading.

491 In a second step we interpret a *FAC*'s lower-limit diameter as an upper-limit *SS*. We do  
492 this by applying a value for the kappa hygroscopicity parameter, which we set at  $\kappa = 0.5$ , and by  
493 applying the kappa-Köhler formula of Petters and Kreidenweis (2007, their Eq. (6)). This  
494 transformation from lower-limit *D* to upper-limit *SS* converts the *FAC* in Fig. 7a to *FAC*(*SS* =  
495 0.41 %) and the *FAC* in Fig. 7b to *FAC*(*SS* = 0.13 %). We also evaluated how a range of the  
496 kappa parameter ( $0.3 < \kappa < 0.7$ ) translates to a range of *SS*. Our upper-limit  $\kappa$  comes from  
497 airborne measurements made over the Southeast Pacific Ocean during summer (Snider et al.,  
498 2017), and our lower-limit  $\kappa$  is the value recommended by Andreae and Rosenfeld (2008) for  
499 simulating aerosol indirect effects over continents.

500 The *FAC*s in Figs. 7a – b are two of the many available from CCOPE. One way to  
501 aggregate these is to calculate a *FAC* for each of the 20 onshore trajectories. For example, if we  
502 select the lower-limit diameter at  $D = 0.055 \mu\text{m}$ , plot numerator values (Eq. (5)) vs denominator  
503 values (Eq. (5)), and fit with the equation  $Y = a \cdot X$ , the “*a*” we derive is the  $FAC(D = 0.055 \mu\text{m})$   
504 for a particular trajectory. *FAC*s calculated in this way, and with lower-limit *D* selected = 0.120  
505  $\mu\text{m}$ , are presented in the seventh columns of Tables 3 and 4. Correlation coefficients presented in  
506 the eighth columns of these tables mostly exceed 0.5. By averaging over the 20 onshore  
507 trajectories, we calculated the overall averages presented at the bottom of the two tables. These  
508 overall averages are  $FAC(D = 0.055 \mu\text{m}) = 0.35 \pm 0.13$  (Table 3) and  $FAC(D = 0.120 \mu\text{m}) = 0.13$   
509  $\pm 0.07$  (Table 4). This decrease of the *FAC* results because a larger lower-limit *D* (Eq. (5)),  
510 implies a smaller numerator (Eq. (5)), and thus a smaller  $FAC(D)$ .

511 What we refer to as *ensemble-averaged FAC*s were derived by selecting from all 20  
512 onshore trajectories the numerator- and denominator-values represented in Eq. (5). The selected  
513 data pairs were fitted in the manner discussed previously. In addition, upper and lower quartile

Deleted: 11

Deleted: The *FAC*s in Figs. 7a – b are two examples of the many available from CCOPE. We derived averaged *FAC*s, corresponding to each of five  $N_{UHSAS}(D)$  sets (corresponding to five selected lower-limit diameters ( $D = 0.055, 0.070, 0.095, 0.120, \text{ and } 0.200 \mu\text{m}$ )), by plotting  $N_{UHSAS}(D)$  versus  $N_{CPC}$  and fitting the data with the equation  $Y = a \cdot X$  where  $Y = N_{UHSAS}(D)$ ,  $X = N_{CPC}$ , and “*a*” is the averaged *FAC*.¶

Averaged *FAC*s are presented in the seventh columns of Tables 3 and 4 where we symbolize these as  $FAC(D = 0.055 \mu\text{m})$  and  $FAC(D = 0.120 \mu\text{m})$ , respectively. Correlation coefficients presented in the eighth columns of these tables mostly exceed 0.5. By averaging over each of the 20 onshore trajectories, and noting that four of these were limited to a time interval shorter than the nominal two hours (Sect. 4.2 and Tables 3 and 4), we calculated the overall averages presented at the bottom of the two tables. These overall averages are  $FAC(D = 0.055 \mu\text{m}) = 0.35 \pm 0.13$  (Table 3) and  $FAC(D = 0.120 \mu\text{m}) = 0.13 \pm 0.07$  (Table 4). This decrease of the *FAC* results because a larger lower-limit *D* (Eq. (2)), implies a smaller  $N_{UHSAS}(D)$ , and thus a smaller  $FAC(D)$ .

Formatted: Font: Not Italic

Deleted: calculated

Deleted: combining

Deleted:  $N_{CPC}$  and  $N_{UHSAS}(D)$  values from all of the onshore trajectories

538 values of the fitted slopes were calculated by applying the technique of Wolfe and Snider (2012;  
539 their Fig. 4d). We evaluated four ensemble-averaged *FACs* corresponding to four selected  
540 diameters ( $D = 0.070, 0.095, 0.120, \text{ and } 0.200 \mu\text{m}$ ). The *FAC* at  $D = 0.055 \mu\text{m}$  was eliminated  
541 from this analysis because Kupc et al. (2018) showed that UHSAS measurements, at  $D \leq 0.070$   
542  $\mu\text{m}$ , are negatively biased. Results are presented as circles in Fig. 8 and vertical error bars  
543 represent the quartile range. Values plotted on the abscissa correspond to the four diameters,  
544 each transformed to an *SS* using the kappa–Köhler formula with  $\kappa = 0.5$ , and horizontal error  
545 bars extend from most hygroscopic ( $\kappa = 0.7$ ), at the left-most limit, to least hygroscopic ( $\kappa =$   
546  $0.3$ ), at the right-most limit.

547 In Fig. 8 we used power laws of the form  $FAC(SS) = C \cdot SS^k$  (i.e., the form commonly used  
548 to parameterize CCN activation spectra (Twomey 1959)) to fit the points. The change in the  
549 slope of the fit function, seen here at  $SS = 0.15\%$ , seems consistent with analyses demonstrating  
550 that in polluted marine cloud conditions, albeit during summertime, the exponent “ $k$ ” in the  
551 Twomey power fit function is  $\geq 1$  and  $\leq 1$  at  $SS < 0.1\%$  and  $SS > 0.1\%$ , respectively (Hudson  
552 and Nobel 2014; data from the MASE project in their Fig. 1).

553 Our parameterized CCN activation spectrum (Fig. 8) is relevant to cloud-aerosol-  
554 precipitation modeling for several reasons. First, some numerical models treat *SS* as a prognostic  
555 variable and thus require initialization with a CCN activation spectrum (e.g., Khairoutdinov and  
556 Kogan 2000). Similarly, some models initialize with a particle size-dependent ASD function and  
557 use Köhler theory to derive a model-initializing CCN activation spectrum (e.g., Lebo et al.  
558 2012). As described in these two references, these models initialize with a nonspecific CCN  
559 activation spectrum. If those models were used to investigate wintertime clouds and precipitation  
560 on the Central Chilean Coast, our parameterization could be applied as a CCOPE-specific

Deleted: -measured concentrations

562 initialization. Second, since we have measurements of  $N_{CPC}$  for the totality of CCOPE (Table 1),  
563 and we have shown how an ensemble-averaged CCN activation spectrum can be developed with  
564  $N_{CPC}$  as the input parameter – i.e. as  $N(SS) = FAC(SS) \cdot N_{CPC}$  – our parameterization can be used  
565 to estimate activation spectra for the complete CCOPE campaign. Third, model initiation with a  
566 specific CCN activation spectrum, as opposed to initialization with a regime-dependent droplet  
567 concentration (e.g., Thompson et al. 2004), is justified by sensitivities to cloud droplet activation  
568 reported in several publications (Cooper et al. 1997; Hudson and Yum, 1997; Snider et al.,  
569 2017).

570 An assumption implicit in our development is that particles were internally mixed within  
571 each of the four particle size classes. This seems justified by our use of HYSPLIT to  
572 conditionally sample (Sect. 3.1), and by the fact that the sampled airmasses were resident in the  
573 marine boundary layer for hours to days while subject to a variety of processes (Brownian  
574 coagulation and reactive uptake of  $SO_2$ , among others) that produce aerosols consistent with the  
575 internal mixture assumption (Fierce et al. 2017). An aspect of our measurements also supports  
576 the internal mixture assumption. Fig. 7b shows that number concentration corresponding to the  
577 0.120 to 1  $\mu m$  class is dominated by particles with diameters at the lower end of that class.  
578 Hence, the contribution of freshly emitted SSA particles, generally thought to size at dry  
579 diameters larger than 0.5  $\mu m$  (Clarke et al. 2003; LS04), and with a  $\kappa = 1.2$  (Berg et al. 1998), is  
580 typically small. A different bias would result if particles with  $\kappa$  values smaller than the lower-  
581 limit value ( $\kappa = 0.3$ ) contributed significantly to the size-integrated concentration in Eq. (5).  
582 Burning biomass is an important source for such low-hygroscopicity particles (Carrico et al.  
583 2005). Our conditional sampling (Sect. 3.1), combined with our filtering of the CPC and UHSAS  
584 measurements (Sect. 3.1 and Appendix B), reduces this concern.

Deleted: the

Deleted: a

Deleted: n  $N_{UHSAS(D)}$  class



#### 588 4.5 Regression of $N_{>0.5}$ and Sea Surface Wind Speed

589 As discussed in Sect. 3.2,  $N_{>0.5}$  represents the concentration of particles larger than 0.5  
590  $\mu\text{m}$ . We now support our conjecture that particles grouped into the  $N_{>0.5}$  subset are indeed SSA.  
591 We do this by analyzing the correlation between  $N_{>0.5}$  and sea surface wind speed ( $U$ ). Sect. 3.1  
592 explains how we used HYSPLIT to derive  $U$ .

593 Values of  $N_{>0.5}$ , corresponding to the 18 sea surface trajectories (Sect. 3.1), are plotted  
594 against  $U$  in Fig. 9. Linear least-squares regression analysis with a model equation of form  
595  $\ln(N_{>0.5}) = \ln(N_o) + a_N \cdot U$  was used to derive the coefficients  $N_o$  and  $a_N$  (O'Dowd and Smith  
596 1993; LS04). The fitted coefficients are  $N_o = 0.15 \text{ cm}^{-3}$  and  $a_N = 0.38$  and the derived function  
597 (black curve) is shown in Fig. 9. The dashed black curves represent the 95% confidence interval  
598 (Romano 1977; his Eq. (4.2.3.f)). Also plotted (pink line) is the function derived by O'Dowd and  
599 Smith (1993) for dried SSA particles with diameter between 0.38 and 0.84  $\mu\text{m}$ . Given that the  
600 O'Dowd and Smith (1993) function (their Fig. 7a) is associated with statistical uncertainty  
601 comparable to what we estimate for our data set, we are only moderately confident that the  
602 function we derived is a consequence of wind-generated SSA. Two caveats require mentioning.  
603 First, a fraction of our data points ( $\sim 25\%$ ) lie either above or below our confidence interval (Fig.  
604 9). Meteorology can contribute to this variability, as when sea surface winds establish a SSA  
605 population, and the wind subsequently slacks, or speeds up, prior to advection onto the continent.  
606 This is expected because the atmospheric residence time of  $D \sim 0.5 \mu\text{m}$  particles, in the absence  
607 of precipitation, is several days (LS04, p. 76). Also, our unintentional sampling of particles  
608 generated over the continent is a concern. We have taken steps to eliminate those sources of  
609 contamination (Sect. 3.1 and Appendix B), but our methods are not foolproof.

#### 610 5 Discussion

Deleted: during ship-based sampling

612 The measurements analyzed here are, to the best of our knowledge, the first to  
613 characterize aerosol microphysical properties on the Central Chilean Pacific coast during winter.  
614 Since the measurement site was relatively close to a population center (Arauco, Chile), and a  
615 SO<sub>2</sub> emitting paper mill, and because wood burning is an important source of residential heat in  
616 this region, we suspect that our measurements are influenced by these land sources. We  
617 mitigated against this by focusing on data collected during periods of onshore flow. Additional  
618 steps were taken to minimize contamination from land-based aerosol sources. These procedures  
619 are explained in Sect. 3.1, 4.2, Appendix B, and in the Supplementary Material.

Deleted: aerosol concentrations and aerosol size distributions

620 A point of comparison is the summertime measurements reported in HK98. Their data  
621 were collected during airborne sampling over the western Atlantic in air that had advected from  
622 the United States. HK98's averaged aerosol surface area ( $131 \pm 93 \mu\text{m}^2 \text{cm}^{-3}$ ; their Table 2) is  
623 clearly larger than that for our 20 onshore trajectories ( $42 \pm 27 \mu\text{m}^2 \text{cm}^{-3}$ ; results not shown).  
624 However, a more relevant comparator would be low altitude measurements made off the Central  
625 Chilean Pacific during winter. As far as we know, the desired data set is not available. Values of  
626 aerosol surface area in the FT over the North and South Pacific are generally  $< 10 \mu\text{m}^2 \text{cm}^{-3}$   
627 (Clarke 1992), suggesting that even during onshore flow the Arauco Site is affected by  
628 anthropogenic sources. We have assumed these sources are Chilean, however, a contribution  
629 from long range transport cannot be ruled out.

Deleted: was

Deleted: measurements are

630 The larger winter-averaged CPC concentration at Arauco, compared to THD, is evidence  
631 for stronger continental contamination at the former. Since  $N_{CPC}$  is a parameter in our  
632 parameterization of CCN activation spectra (Sect. 4.4), we conclude that cloud droplet  
633 concentrations in low level marine clouds (stratocumulus) formed in the vicinity of Arauco are  
634 larger than in similar clouds near THD. If true, this conclusion would be opposite the general

Deleted: time

Deleted: Arauco

640 situation in Southern Pacific boundary layer clouds where cloud droplet concentrations are  
641 statistically less than in their Northern hemispheric counterparts (Bennartz 2007). Relevant to  
642 this, Bennartz (2007) comments on a coast-normal droplet concentration gradient that is stronger  
643 on the Central Chilean coast compared to the California/Oregon coast. We presume that the  
644 gradient exists because of the larger concentration of aerosols over continents (Andreae and  
645 Rosenfeld, 2008), and because of aerosol removal that occurs within and below marine  
646 stratocumulus clouds. In addition, Bennartz (2007) demonstrates that the coast-normal droplet  
647 concentration gradient is larger off the Central Chilean coast, compared to California/Oregon  
648 coast, in part because oceanic concentrations, ~ 2000 km offshore, are generally smaller in the  
649 south compared to the north Pacific. Whether the southern hemispheric gradient is also enhanced  
650 by larger aerosol concentrations over coastal Central Chile, compared to coastal California and  
651 Oregon, is an open question. Further analysis of the satellite retrievals analyzed by Bennartz  
652 (2007), with segregation into wintertime and summertime categories, as well as measurements  
653 conducted at an offshore island location, or acquired using aircraft or ships, are needed to  
654 address this question.

Deleted: resolve

655

657 **6 Conclusions**

658           Analyses presented here are based on Condensation Particle Counter (CPC)  
659 measurements made during one winter season (June, July and August 2015) on the Central  
660 Chilean Pacific coast (38 ° S). Also analyzed are aerosol size distribution measurements made  
661 with an Ultra High Sensitivity Aerosol Spectrometer (UHSAS). UHSAS measurements are  
662 available from 29 May to 28 June (Table 1). Limitations of this study are proximity of the  
663 measurement site to a population center (Arauco, Chile) and a SO<sub>2</sub> emitting paper mill, sampling  
664 of particles emitted from residences close to where our instruments were operated, and the  
665 incomplete drying of the sampled aerosol particles. This first attempt to make CPC and ASD  
666 measurements on the Central Chilean Pacific coast during winter was exploratory and our results  
667 should be considered preliminary.

668           We compared CPC-measured concentrations from the Arauco Site to values acquired at  
669 the NOAA observatory Trinidad Head (THD) on the North Pacific Coast of California. The  
670 averaged CPC concentration is larger at the Arauco Site and that difference is evident in an  
671 Arauco/THD comparison based on air arriving from all wind directions and from clean sector  
672 directions. In addition, we conditionally sampled UHSAS-measured size distributions and  
673 derived parameterized descriptions of sea salt aerosol (SSA) and cloud condensation nuclei  
674 (CCN) for periods of onshore flow. In these parameterizations the input parameters are  
675 respectively sea surface wind speed and CPC-measured concentration.▼

676           In the context of CCOPE, there are two precipitation regimes that impact the Central  
677 Chilean Coast and the Nahuelbuta Mountains during winter (Massmann et al. 2017). The first of  
678 these have radar-derived echo tops at ~ 2 km MSL and produce rain by direct conversion of  
679 cloud droplets to rain drops. The second have higher echo tops, extending to temperatures colder

**Deleted:** We compared the Arauco Site CPC measurements to values acquired at the NOAA observatory Trinidad Head (THD) on the North Pacific Coast of California. Averaged CPC concentrations are larger at the Arauco Site and that difference is evident in Arauco/THD comparisons based on air arriving from all wind directions and from clean sector directions. In addition, we conditionally sampled the UHSAS measurements and derived parameterized descriptions of sea salt aerosol (SSA) and cloud condensation nuclei (CCN) for periods of onshore flow. In these parameterizations the input parameters are respectively sea surface wind speed and CPC-measured aerosol concentration.

691 than 0 °C and produce rain that is, at least in part, initiated by ice phase processes. Investigation  
692 of the rain produced in the shallow regimes is an active area research; it is thought that SSA and  
693 the CCN play important roles (Feingold et al. 1999; Gerber and Frick 2012). The deep regimes  
694 form precipitating hydrometeors (ice particles) at cloud temperatures < 0 °C. Again, aerosols  
695 play a role, but there are many facets to this and first-order effects are not yet agreed on. Perhaps  
696 foremost is the role played by aerosol acting as ice nuclei. Measurement of an ice nuclei  
697 activation spectrum, development of an ice particle parameterization, and incorporation of the  
698 parameterization into a numerical model are needed to explore this dimension of the problem.  
699 Because they modulate cloud droplet size, the development of graupel, and influence latent  
700 heating (e.g., Tao et al. 2012), the CCN and SSA likely also play a role in the deep regimes.  
701 Thus, we anticipate that modeling of both precipitation regimes will benefit from the CCN and  
702 SSA parameterizations presented here.

703 **Author Contribution**

704           Jeff Snider, Jason Minder, David Kingsmill wrote successful proposals that funded this  
705 research. Sara Fults, Adam Massman, Aldo Montecinos, and David Kingsmill performed the  
706 field measurements. Rene´ Garraud and Aldo Montecinos provided logistical support during the  
707 field phase of the project. Elisabeth Andrews provided data from THD. Sara Fults wrote her MS  
708 dissertation and this was adapted to this manuscript by Jeff Snider. All authors contributed to the  
709 editing of this manuscript.

710 **Acknowledgments**

711           We thank Freddy Echeverría-Cabezas for his assistance during CCOPE, Matthew  
712 Burkhart for building the aerosol data acquisition system, Zhien Wang for providing a graduate  
713 assistantship, Nicholas Mahon for shipping logistics, and the Departamento de Geofísica at the  
714 Universidad de Concepción. This work was supported by the United States National Science  
715 Foundation Physical and Dynamic Meteorology Division under Awards AGS-1522277 and  
716 AGS-1522939.

717 **Data Availability**

718           CCOPE CPC and UHSAS data, and a data reader (Interactive Data Language, Harris  
719 Geospatial Solutions, Inc.), are at <http://www-das.uwyo.edu/~jsnider/CCOPE/>.

720

721 **Appendix A.**

722 Because the *RH* at the Arauco Site was often in excess of 80 % (Fig. A1c), particles  
723 entering the sample tube (Sect. 2.2) were haze droplets (Rogers and Yau 1989). As these haze  
724 droplets transit the sample tube they experience an increase in temperature, an *RH* decrease, and  
725 thus a decreased *D*. The lowest *RH* experienced by a haze droplet is at the point of detection  
726 where the aerosol temperature is presumed to be the internal “box temperature” measured by the  
727 UHSAS. The *RH* at this point is

$$RH_U = \frac{RH_A \cdot e_s(T_A)}{e_s(T_U)} \quad (A1)$$

729 where  $T_U$  is the internal UHSAS temperature,  $e_s$  is saturation vapor pressure (temperature  
730 dependent), and  $RH_A$  and  $T_A$  are the ambient *RH* and temperature, respectively. In nearly all of  
731 the UHSAS sampling during CCOPE, the  $RH_U$  was less than 60 % (Fig. A1d). This suggests that  
732 the haze droplets detected by the UHSAS were partially dried. Partial drying of the haze droplets  
733 is supported by calculations (Lewis and Schwartz 2004; their Fig. 8) showing that a  $D = 4 \mu\text{m}$   
734 NaCl haze droplet reaches its equilibrium size ( $D = 2 \mu\text{m}$ ) in 0.1 s subsequent to a step-change of  
735 *RH* from 98 % to 80 %. Because 0.1 s is small relative to the average residence time of haze  
736 droplets within the sample tube (0.8 s), we ignored the possibility of a kinetic limitation to drying  
737 and we assumed that the haze droplets relaxed to their equilibrium size at  $RH_U$  prior to the time  
738 they were detected. Since we do not know the chemical composition of the haze droplets, their  
739 equilibrium size is uncertain, but calculations corresponding to  $RH_U = 60\%$  and a haze droplet  
740 composed of sodium sulfate indicate that the equilibrium size is 30% larger than the  
741 corresponding dry particle size (Snider et al. 2017; their Fig. A2b). Three factors interact to  
742 partially compensate for a size overestimate due to incomplete particle drying; 1) Particle sizing

Deleted: :

Deleted: thermodynamic

Deleted: not specifiable

Deleted: during CCOPE

747 performed by the UHSAS was calibrated using polystyrene latex particles (refractive index  $n =$   
748  $1.57$  at  $\lambda = 1.05 \mu\text{m}$  (Marx and Mulholland 1983)); 2) Liquid water ( $n = 1.32$  at  $\lambda = 1.05 \mu\text{m}$   
749 (Irvine and Pollack, 1968)) makes a significant contribution to the mass of a haze droplet at  $RH =$   
750  $60\%$  (here again we are assuming the above-mentioned sodium sulfate composition for the  
751 completely dried particle); and 3) Assuming the same scattering intensity, an  $n = 1.6$  particle  
752 sizes  $10\%$  smaller than an  $n = 1.4$  particle (Cai et al., 2008; their Fig. 1). Accepting the  $10\%$  as  
753 an underestimate, and the above-mentioned  $30\%$  as an overestimate, we conclude that particle  
754 sizes reported by the UHSAS were overestimated by  $20\%$ . We did not correct for this sizing bias.

755 Laboratory testing of the UHSAS and CPC is documented in Figs. A2a – b, and in Figs.  
756 A3a - b. We evaluated consistency among measurements made with the UHSAS, the CPC, and a  
757 Scanning Mobility Particle Scanner (SMPS; TSI 2000b). In all of these tests, the  $RH$  of the test  
758 aerosols was  $< 15 \%$ . An example ASD derived using the UHSAS (pink) and the SMPS (black)  
759 is shown in Fig. A2a. In this test the three instruments (UHSAS, CPC and SMPS) were sampling  
760 mobility-selected ammonium sulfate particles with  $D = 0.075 \mu\text{m}$ . The refractive index of this  
761 material at  $\lambda = 1.05 \mu\text{m}$  is  $n = 1.51$  (Toon et al., 1976). It is evident that the mode diameter  
762 measured by the UHSAS is smaller than that reported by the SMPS ( $D = 0.075 \mu\text{m}$ ). This  
763 difference is qualitatively consistent with the smaller refractive index of the test material  
764 (ammonium sulfate), compared to the larger refractive index of the polystyrene latex particles  
765 used by the factory to calibrate the UHSAS (DMT, 2013). Fig. A2b shows a test with  $D = 0.71$   
766  $\mu\text{m}$  polystyrene latex particles. As expected, the mode diameter in the UHSAS size distribution  
767 is in agreement with the mode size in the SMPS size distribution.

768 An additional feature of our laboratory testing is the multi-modal structure in the SMPS  
769 size distribution at  $D < 0.5 \mu\text{m}$  (Fig A2b). This structure results because the particle diameter



770 inferred by the SMPS depends on the physical diameter of the test particles, and on also depends  
771 on the test particle's charge state. The multi-modal structure at  $D < 0.5 \mu\text{m}$  corresponds to  
772 particles carrying 5, 4, 3, and 2 fundamental charges, but each with physical diameter equal 0.71  
773  $\mu\text{m}$ . As stated in the previous paragraph, the latter is the diameter of the polystyrene test  
774 particles.

775 Figs. A3a - b summarize all of the lab testing we conducted in support of CCOPE. In Fig.  
776 A3a,  $N_{UHSAS}$  is plotted vs  $N_{CPC}$  for tests with  $D < 0.2 \mu\text{m}$  and Fig. A3b has tests with  $D > 0.2 \mu\text{m}$ .  
777 On average, concentrations differ by  $\pm 6 \%$  in Fig. A3a ( $D < 0.2 \mu\text{m}$ ) and by  $\pm 10 \%$  in Fig. A3b  
778 ( $D > 0.2 \mu\text{m}$ ).

779

780 **Appendix B,**

781 For each of the onshore trajectories (Sect. 3.1), a two-hour segment, centered on the  
782 trajectory arrival time was analyzed. An example is in Figs. B1a – e. The first panel (Fig. B1a)  
783 shows the sequence of CPC values sampled every second (i.e., 1-s samples referred to as *fast*  
784 *N<sub>CPC</sub>*), and Fig. B1b shows CPC values sampled every 10 seconds (i.e., 10-s samples referred to  
785 as *slow N<sub>CPC</sub>*). The following procedure was used to attenuate the narrow perturbations that were  
786 likely the result of local aerosol emissions (e.g., within the time interval indicated by vertical  
787 dashed lines in Figs. B1a, B1b, and B1d).

788 First, the fast *N<sub>CPC</sub>* values were used to determine, for each 10 s of the sequence, a  
789 concentration relative standard deviation ( $\sigma / \langle x \rangle$ ). Second, if the relative standard deviation was  
790 greater than 0.02 both the slow *N<sub>CPC</sub>* measurement (sampled once every 10 second) and the ASD  
791 measurement (also sampled once every 10 second; Table 1) were discarded. Fig. B1c and Fig.  
792 B1e show the *N<sub>CPC</sub>* and *N<sub>UHSAS</sub>* sequences after application of the filter. These two filtered  
793 sequences (*N<sub>CPC</sub>*(filtered) and *N<sub>UHSAS</sub>*(filtered)), and the filtered values of aerosol surface area  
794 (*S<sub>UHSAS</sub>*), aerosol volume (*V<sub>UHSAS</sub>*), and *D* > 0.5  $\mu\text{m}$  concentration (*N<sub>>0.5</sub>*) are the focus of the bulk  
795 of our analysis.

Deleted: :

**Deleted:** For each of the onshore trajectories (Sect. 3.1), a two-hour segment, centered on the trajectory arrival time was analyzed. An example is in Figs. B1a – e. Fig. B1a shows the sequence of CPC values sampled every second (i.e., 1-s samples referred to as *fast N<sub>CPC</sub>*), and Fig. B1b shows CPC values sampled every 10 seconds (i.e., 10-s samples referred to as *slow N<sub>CPC</sub>*). The following procedure was used to attenuate the narrow perturbations (e.g., within the time interval indicated by vertical dashed lines in Figs. B1a, B1b, and B1d) that were likely the result of local aerosol emissions.

808 **References**

- 809 Albrecht, B. A., Aerosols, cloud microphysics, and fractional cloudiness, *Science*, 245, 1227 –  
810 1230, 1989
- 811
- 812 Andreae, M.O., Correlation between cloud condensation nuclei concentration and aerosol optical  
813 thickness in remote and polluted regions, *Atmos. Chem. Phys*, 9, 543-556, 2009
- 814
- 815 Andreae, M.O. and D. Rosenfeld, Aerosol-cloud-precipitation interactions. Part 1. The nature  
816 and sources of cloud-active aerosols, *Earth-Sci. Rev.*, 89, 13 – 41, 2008
- 817
- 818 Arauco Woodpulp, accessed 16 December 2018 at:  
819 [http://web.arauco.cl/\\_file/file\\_3382\\_pulp%20catalog.pdf](http://web.arauco.cl/_file/file_3382_pulp%20catalog.pdf), 2010
- 820
- 821 Bennartz, R., Global assessment of marine boundary layer cloud droplet number concentration  
822 from satellite, *J. Geophys. Res.*, 112, D02201, 2007
- 823
- 824 Berg, O. H., E. Swietlicki, and R. Krejci, Hygroscopic growth of aerosol particles in the marine  
825 boundary layer over the Pacific and Southern Oceans during the First Aerosol  
826 Characterization Experiment (ACE 1), *J. Geophys. Res.*, 103, 16535-16545, 1998
- 827
- 828 Birmili, W., A. Wiedensohler, J. Heintzenberg, and K. Lehmann, Atmospheric particle number  
829 size distribution in central Europe: Statistical relations to air masses and meteorology, *J.*  
830 *Geophys. Res. Atmos.*, 106, 32005–32018, 2001
- 831
- 832 Boucher, O., and Coauthors, Clouds and Aerosols. In: *Climate Change 2013: The Physical*  
833 *Science Basis. Contribution of Working Group I to the Fifth Assessment Report of the*  
834 *Intergovernmental Panel on Climate Change* [Stocker, T.F., D. Qin, G.-K. Plattner, M.  
835 Tignor, S.K. Allen, J. Boschung, A. Nauels, Y. Xia, V. Bex and P.M. Midgley (eds.)],  
836 Cambridge University Press, Cambridge, United Kingdom, 2013
- 837
- 838 Brechtel, F. J., S. M. Kreidenweis, and H. B. Swan, Air mass characteristics, aerosol particle  
839 number concentrations, and number size distributions at Macquarie Island during the  
840 First Aerosol Characterization Experiment (ACE 1), *J. Geophys. Res. Atmos.*, 103,  
841 16351–16367, 1998
- 842
- 843 Cai, Y., J.R. Snider and P. Wechsler, Calibration of the passive cavity aerosol spectrometer  
844 probe for airborne determination of the size distribution, *Atmos. Meas. Tech.*, 6, 2349-  
845 2358, 2013
- 846
- 847 Cai, Y., D.C.Montague, W.Mooiweer-Bryan and T.Deshler, Performance characteristics of the  
848 ultra high sensitivity aerosol spectrometer for particles between 55 and 800 nm:  
849 Laboratory and field Studies, *J.Aerosol Sci.*, 39, 759-769, 2008
- 850

851 Carrico, C.M., S.M.Kreidenweis, W.C.Malm, D.E.Day, T.Lee, J.Carrillo, G.R.McMeeking, J.L.  
852 Collett, Hygroscopic growth behavior of a carbon-dominated aerosol in Yosemite  
853 National Park, *Atmos. Environ.*, 39, 1393-1404, 2005  
854  
855 Clarke, A., Atmospheric Nuclei in the Remote Free-Troposphere, *J. Atmos. Chem.*, 14, 479-488,  
856 1992  
857 Clarke, A., V. Kapustin, S. Howell, K. Moore, B. Lienert, S. Masonis, T. Anderson, and D.  
858 Covert, Sea-salt size distribution from breaking waves: Implications for marine aerosol  
859 production and optical extinction measurements during SEAS, *J. Atmos. Ocean.  
860 Technol.*, 20, 1362–1374, 2003  
861  
862 Cooper, W.A., R.T. Bruintjes, and G.K. Mather, Calculations pertaining to hygroscopic seeding  
863 with flares, *J. Appl. Meteor.*, 36, 1449 – 1469, 1997  
864  
865 Covert, D. S., V. N. Kapustin, P. K. Quinn, and T. S. Bates, New particle formation in the  
866 marine boundary layer, *J. Geophys. Res.*, 97(D18), 20581–20589,  
867 doi:10.1029/92JD02074, 1992  
868  
869 Dall’Osto, M., and Coauthors, Aerosol properties associated with air masses arriving into the  
870 North East Atlantic during the 2008 Mace Head EUCAARI intensive observing period:  
871 an overview, *Atmos. Chem. Phys. Discuss.*, 9, 26265–26328, 2009  
872  
873 Diesch, J. M., F. Drewnick, S. R. Zorn, S. L. Von Der Weiden-Reinmüller, M. Martinez, and S.  
874 Borrmann, Variability of aerosol, gaseous pollutants and meteorological characteristics  
875 associated with changes in air mass origin at the SW Atlantic coast of Iberia, *Atmos.  
876 Chem. Phys.*, 12, 3761-3782, 2012  
877  
878 DMT, Ultra High Sensitivity Aerosol Spectrometer (UHSAS) Operator Manual, Boulder, CO,  
879 2013  
880  
881 Feingold, G., W. R. Cotton, S. M. Kreidenweis, J. T. Davis, and J. A. T. D. Avis, The Impact of  
882 Giant Cloud Condensation Nuclei on Drizzle Formation in Stratocumulus: Implications  
883 for Cloud Radiative Properties, *J. Atmos. Sci.*, 56, 4100–4117, 1999  
884  
885 Fierce, L., N. Riemer, and T.C. Bond, Toward Reduced Representation of Mixing State for  
886 Simulating Aerosol Effects on Climate. *Bull. Amer. Meteor. Soc.*, 98, 971–980,  
887 <https://doi.org/10.1175/BAMS-D-16-0028.1>, 2017  
888  
889 Fults, S., Aerosol measurements during the Central Chilean Orographic Precipitation  
890 Experiment, M.S. Thesis, Department of Atmospheric Science, University of Wyoming,  
891 2016  
892  
893 Garreaud, R., M.Falvey, and A.Montecinos, Orographic precipitation in coastal southern Chile:  
894 Mean distribution, temporal variability, and linear contribution, *J. Hydrometeor.*, 1185 –  
895 1202, 2016  
896

- 897 Gerber, H. and G.Frick, Drizzle rates and large sea-salt nuclei in small cumulus, J. Geophys.  
898 Res., 117, D01205, 2012  
899
- 900 Gras, J.L., Baseline atmospheric condensation nuclei at Cape Grim 1977-1987, J. Atmos. Chem.,  
901 11, 89-106, 1990  
902
- 903 Gras, J. L., CN, CCN and particle size in Southern Ocean air at Cape Grim, J. Atmos. Res.,  
904 35, 233–251, 1995  
905
- 906 Hansen, J., The Faustian Bargain: Humanity's Own Trap, Storms of My Grandchildren,  
907 Bloomsbury, 320 pp., 2009  
908
- 909 Havlicek, L.L., and R.D. Crain, Practical Statistics for the Physical Sciences, American  
910 Chemical Society, 512 pp., 1988  
911
- 912 Hegg, D. A., and Y. J. Kaufman, Measurements of the relationship between submicron aerosol  
913 number and volume concentration, J. Geophys. Res., 103, 5671-5678, 1998  
914
- 915 Hinds, W. C., Aerosol Technology: Properties, Behavior and Measurement of Airborne  
916 Particles, John Wiley & Sons, INC, 483, 1999  
917
- 918 Hoppel, W. a., G. M. Frick, J. W. Fitzgerald, and R. E. Larson, Marine boundary layer  
919 measurements of new particle formation and the effects nonprecipitating clouds have, J.  
920 Geophys. Res., 99, 14443–14459, 1994  
921
- 922 Hudson, J.G. and S. Yum, Droplet spectral broadening in marine stratus. J. Atmos. Sci., 54,  
923 2642–2654, 1997  
924
- 925 Hudson, J.G., and S.Nobel, CCN and vertical velocity influences on droplet concentrations and  
926 supersaturations in clean and polluted stratus clouds, J. Atmos. Sci., 312-331, 2014  
927
- 928 Hudson, J.G., S.Noble, and S.Tabor, Cloud supersaturations from CCN spectra Hoppel minima,  
929 J. Geophys. Res. Atmos., 120, 3436–3452, doi:10.1002/2014JD022669, 2015  
930
- 931 [International Civil Aviation Organization \(ICAO\), Manual of the ICAO Standard Atmosphere:  
932 extended to 80 kilometres \(262 500 feet\), 3rd ed., ISBN-92-9194-004-6, 1993](#)  
933
- 934 Irvine, W.M. and J.B. Pollack, Infrared optical properties of water and ice spheres, Icarus, 8, 324  
935 – 360, 1968  
936
- 937 Khairoutdinov, M. and Y. Kogan, A new cloud physics parameterization in a large-eddy  
938 simulation model of marine stratocumulus, Mon. Wea. Rev., 128, 229 - 243, 2000  
939
- 940 Kupc, A., Williamson, C., Wagner, N. L., Richardson, M., and Brock, C. A.: Modification,  
941 calibration, and performance of the Ultra-High Sensitivity Aerosol Spectrometer for  
942 particle size distribution and volatility measurements during the Atmospheric

Formatted: Indent: Left: 0", Hanging: 0.5"

943 Tomography Mission (ATom) airborne campaign, *Atmos. Meas. Tech.*, 11, 369-383,  
944 <https://doi.org/10.5194/amt-11-369-2018>, 2018  
945  
946 Lebo, Z. J., Morrison, H., and Seinfeld, J. H., Are simulated aerosol-induced effects on deep  
947 convective clouds strongly dependent on saturation adjustment?, *Atmos. Chem. Phys.*,  
948 12, 9941-9964, 2012  
949  
950 Lewis, E. R., and S. E. Schwartz, *Sea Salt Aerosol Production: Mechanisms, Methods,*  
951 *Measurements, and Models*, American Geophysical Union, 413 pp., 2004  
952  
953 Marx, E. and G.W. Mulholland, Size and refractive index determination of single polystyrene  
954 spheres, *Journal of Research of the National Bureau of Standards*, 88, 321 – 338, 1983  
955  
956 Massmann, A.K., J.R. Minder, R.D. Garreaud, D.E. Kingsmill, R.A. Valenzuela, A. Montecinos,  
957 S.L. Fuels, and J.R. Snider, 2017, The Chilean Coastal Orographic Precipitation  
958 Experiment: Observing the Influence of Microphysical Rain Regimes on Coastal  
959 Orographic Precipitation. *J. Hydrometeor.*, 18, 2723–2743, [https://doi.org/10.1175/JHM-](https://doi.org/10.1175/JHM-D-17-0005.1)  
960 [D-17-0005.1](https://doi.org/10.1175/JHM-D-17-0005.1), 2017  
961  
962 McMurry, P.H., X.Wang, K.Park, and K.Ehara, The relationship between mass and mobility for  
963 atmospheric particles: A new Technique for measuring particle density, *Aerosol Sci.*  
964 *Technol.*, 36, 227–238, 2002  
965  
966 McCoy, D.T., D.L. Hartmann, and D.P. Grosvenor, Observed Southern Ocean Cloud Properties  
967 and Shortwave Reflection. Part I: Calculation of SW Flux from Observed Cloud  
968 Properties. *J. Climate*, 27, 8836–8857, <https://doi.org/10.1175/JCLI-D-14-00287.1>, 2014  
969  
970 NOAA, HYSPLIT Trajectory Model, NOAA Air Resources Laboratory, Silver Spring, MD,  
971 Accessed 1 August 2016, [Available online at <https://ready.arl.noaa.gov/HYSPLIT.php>],  
972 2016  
973  
974 O’Dowd, C.D., and M.H. Smith, Physicochemical properties of aerosols over the Northeast  
975 Atlantic: evidence for wind-speed-related submicron sea-salt aerosol production,  
976 *J. Geophys. Res.*, 98, 1137-1149, 1993  
977  
978 Petters, M. D., J. R. Snider, B. Stevens, G. Vali, I. Faloona, and L. M. Russell, Accumulation  
979 mode aerosol, pockets of open cells, and particle nucleation in the remote subtropical  
980 Pacific marine boundary layer, *J. Geophys. Res. Atmos.*, 111, 1–15, 2006  
981  
982 Petters, M. D., and S. M. Kreidenweis, A single parameter representation of hygroscopic growth  
983 and cloud condensation nucleus activity. *Atmos. Chem. Phys.*, 7, 1961–1971, 2007  
984  
985 Raes, F., R. Van Dingenen, E. Cuevas, P. F. J. Van Velthoven, and J. M. Prospero, Observations  
986 of aerosols in the free troposphere and marine boundary layer of the subtropical  
987 Northeast Atlantic: Discussion of processes determining their size distribution, *J.*  
988 *Geophys. Res.*, 102, 21315, 1997

989  
990 Rogers, R. R., and M. K. Yau, A Short Course in Cloud Physics. 3rd ed. Pergamon Press, 304  
991 pp., 1989  
992  
993 Romano, A., Applied Statistics for Science and Industry, Allyn and Bacon Inc., pp. 385, 1977  
994  
995 Schwartz, S.E., Are global cloud albedo and climate controlled by marine phytoplankton?,  
996 Nature, 336, 441-445, 1988  
997  
998 Snider, J.R., D.Leon and Z.Wang, Droplet Concentration and Spectral Broadening in Southeast  
999 Pacific Stratocumulus, J. Atmos. Sci., 74, 719-749, 2017  
1000  
1001 Tao, W.-K., J.-P. Chen, Z. Li, C. Wang, and C. Zhang, Impact of aerosols on convective clouds  
1002 and precipitation, Rev. Geophys., RG2001, 2012  
1003  
1004 Thompson, G., R.M. Rasmussen and K. Manning, Explicit forecasts of winter precipitation using  
1005 an improved bulk microphysics scheme. Part I: Description and sensitivity analysis, Mon.  
1006 Weather Rev., 132, 519 – 542, 2004  
1007  
1008 Toon, O.B., The optical constants of several atmospheric aerosol species: Ammonium sulfate,  
1009 aluminum oxide, and sodium chloride, J. Geophys. Res., 81, 5733 - 5748, 1976  
1010  
1011 TSI, Inc., Condensation Particle Counter Instruction Manual, St. Paul, Minnesota, 2000a  
1012  
1013 TSI, Inc., Model 3080 Electrostatic Classifier Instruction Manual, St. Paul, Minnesota, 2000b  
1014  
1015 Twomey, S., Pollution and the Planetary Albedo, Atmospheric Environment, 8, 1251–56, 1974  
1016  
1017 Twomey, S., The nuclei of natural cloud formation part II: The supersaturation in natural clouds  
1018 and the variation of cloud droplet concentration, Geofis. Pura Appl., 43, 243-249, 1959  
1019  
1020 van Dingenen, R., A. O. Virkkula, F. Raes, T. S. Bates, A. Wiedensohler, A simple non linear  
1021 analytical relationship between aerosol accumulation number and sub-micron volume,  
1022 explaining their observed ratio in the clean and polluted marine boundary layer, Tellus,  
1023 52B, 439-451, 2000  
1024  
1025 [A. Wiedensohler, D. Orsini, D. S. Covert, D. Coffmann, W. Cantrell, M. Havlicek, F. J.](#)  
1026 [Brechtel, L. M. Russell, R. J. Weber, J. Gras, J. G. Hudson & M. Litchy,](#)  
1027 [Intercomparison Study of the Size-Dependent Counting Efficiency of 26 Condensation](#)  
1028 [Particle Counters, Aerosol Science and Technology, 27:2, 224-242. DOI:](#)  
1029 [10.1080/02786829708965469, 1997](#)  
1030  
1031 Wolfe, J. P., and J. R. Snider, 2012: A relationship between reflectivity and snow rate for a high-  
1032 altitude S-band radar, J. Appl. Meteor. Climatol., 51, 1111–1128, 2012  
1033

**Deleted:** TSI Inc., accessed 19 December 2018 at:  
[https://www.artisanng.com/info/PDF\\_5453495F33373630415F333736325F446174617368656574.pdf](https://www.artisanng.com/info/PDF_5453495F33373630415F333736325F446174617368656574.pdf), 1996¶

1038 Yum, S. S., and J. G. Hudson, Wintertime/summertime contrasts of cloud condensation nuclei  
1039 and cloud microphysics over the Southern Ocean, *J. Geophys. Res.*, 109, 1-14, 2004  
1040



1041 Table 1. Aerosol Instruments

Instrument and Reference	Aerosol Property Measured	Particle Diameter Range, $\mu\text{m}$	Aerosol Flow Rate, $\text{cm}^3 \text{s}^{-1}$	Data Acquisition Rate, Hz	Data Availability (2015)
CPC Model 3010 (TSI 2000a)	Aerosol Concentration	$D > 0.012$	17	1	29 May to 14 Aug
UHSAS (DMT 2013)	Aerosol Size Distribution	$0.055 < D < 1$	0.34	0.1	29 May to 28 June

Deleted: 0  
 Deleted: and¶  
 0.1

1042

1043

1047 Table 2. Classification of Air Mass Type

Citation and Location	Measurement Site Characteristics	Air Mass Classification	Averaged CPC Concentration, $\text{cm}^{-3}$ <sup>a</sup>
Gras (1990) Cape Grim, Tasmania 40.68 °S; 144.7 °E	Oceanic Wintertime	Remote Marine	100
Brechtel et al. (1998) Macquarie Island (Southwest Pacific) 54.50 °S; 159.0 °E	Oceanic Summertime	Remote Marine	700
Diesch et al. (2012) Portugal 37.11 °N; 7.735 °W	Coastal Continental Late Autumn	Moderately-polluted Marine Heavily-polluted Marine Continental	1000 7000 10000
This Study Arauco, Chile 37.25 °S; 73.34 °W	Coastal Continental Wintertime	Between moderately-polluted Marine and Heavily-polluted Marine	3000
This Study Trinidad Head, CA 41.05 °N; 124.2 °W	Coastal Continental Wintertime	Moderately-polluted Marine	1000

1048

1049 <sup>a</sup> Values rounded to one significant digit

1050

1051 Table 3. Statistics for Onshore Trajectories ( $D$  integration in Eq. (2), (4), and (5) is from 0.055 to 1  $\mu\text{m}$ )

Arrival Hour, UTC	Type	Start DDHHMM <sup>a</sup> , UTC	End DDHHMM <sup>a</sup> , UTC	$N_{UHSAS}$ on $V_{UHSAS}$ Slope, $\mu\text{m}^{-3}$	$r$ <sup>b</sup>	$FAC(D=0.055 \mu\text{m})$	$r_v$	Number of Samples
06	Sea Surface	050500	050700	93.	0.54	0.59	0.65	139
12	Sea Surface	051100	051134	64.	0.10	0.19	0.59	63
18	Sea Surface	051700	051900	110.	0.66	0.41	0.63	342
00	Sea Surface	052300	060100	298.	0.81	0.51	0.96	316
06	Sea Surface	060500	060700	60.	0.53	0.18	0.89	677
12	Sea Surface	061100	061300	91.	0.60	0.16	0.65	647
18	Sea Surface	061700	061900	107.	0.33	0.18	0.81	476
00	Sea Surface	062300	062325	234.	0.81	0.36	0.97	133
06	Sea Surface	080500	080700 <sup>c</sup>	163.	0.06	0.29	0.52	542
12	Sea Surface	081100	081300	358.	0.75	0.28	0.76	504
18	Sea Surface	081700	081900	450.	0.88	0.42	0.90	416
00	Sea Surface	090020	090033	764.	0.45	0.34	0.98	72
06	Sea Surface	090500	090700	703.	0.68	0.23	0.96	554
12	Sea Surface	091100	091300	714.	0.89	0.44	0.94	532
18	Sea Surface	091700	091900	675.	0.78	0.39	0.53	592
00	Sea Surface	092300	100100	519.	0.37	0.22	0.68	618
06	Aloft	100500	100700	857.	0.96	0.39	0.82	617
18	Sea Surface	101700	101900	825.	0.86	0.37	0.19	622
00	Sea Surface	110006	110031	834.	0.96	0.50	0.99	61
00	Aloft	262300	270100	420.	0.68	0.47	0.93	647
			<x>	417		0.35		
			$\sigma$	297		0.13		
			$\sigma / <x>$	0.71		0.36		

<sup>a</sup> DDHHMM indicates the start and end times (day in June 2015, hour, minute) of the data segment

<sup>b</sup> Pearson product moment for the  $N_{UHSAS}(D=0.055 \mu\text{m})$  on  $V_{UHSAS}(D=0.055 \mu\text{m})$  correlation

<sup>c</sup> Data recording ended at DDHHMM = 080646, i.e., 14 min before the stated end time

Deleted: and

Deleted: <sup>c</sup>

Deleted: <sup>d</sup>

Deleted: <sup>f</sup>

<sup>c</sup> Pearson product moment for the  $N_{UHSAS}(D=0.055 \mu\text{m})$  on  $N_{CRC}$  correlation

Deleted: <sup>d</sup>

1053  
1054  
1055  
1056

1064 Table 4. Statistics for Onshore Trajectories ( $D$  integration in Eq. (2), (4), and (5)) is from 0.120 to 1  $\mu\text{m}$ )

Arrival Hour, UTC	Type	Start DDHHMM <sup>a</sup> , UTC	End DDHHMM <sup>a</sup> , UTC	$N_{UHSAS}$ on $V_{UHSAS}$ Slope, $\mu\text{m}^{-3}$	$r$ <sup>b</sup>	$FAC(D=0.120 \mu\text{m})$	$r_v$	Number of Samples
06	Sea Surface	050500	050700	60.	0.74	0.37	0.47	139
12	Sea Surface	051100	051134	40.	0.31	0.12	0.36	63
18	Sea Surface	051700	051900	64.	0.76	0.23	0.49	342
00	Sea Surface	052300	060100	113.	0.84	0.17	0.84	316
06	Sea Surface	060500	060700	34.	0.67	0.10	0.78	677
12	Sea Surface	061100	061300	44.	0.77	0.07	0.42	647
18	Sea Surface	061700	061900	42.	0.61	0.06	0.24	476
00	Sea Surface	062300	062325	107.	0.93	0.15	0.92	133
06	Sea Surface	080500	080700 <sup>c</sup>	89.	0.72	0.12	0.02	542
12	Sea Surface	081100	081300	139.	0.79	0.09	0.53	504
18	Sea Surface	081700	081900	202.	0.92	0.17	0.83	416
00	Sea Surface	090020	090033	184.	0.12	0.06	0.78	72
06	Sea Surface	090500	090700	228.	0.58	0.06	0.87	554
12	Sea Surface	091100	091300	262.	0.92	0.14	0.73	532
18	Sea Surface	091700	091900	257.	0.89	0.12	0.41	592
00	Sea Surface	092300	100100	204.	0.83	0.06	0.32	618
06	Aloft	100500	100700	323.	0.96	0.11	0.82	617
18	Sea Surface	101700	101900	279.	0.91	0.10	0.08	622
00	Sea Surface	110006	110031	346.	0.97	0.16	0.96	61
00	Aloft	262300	270100	171.	0.65	0.18	0.88	647
			<x>	159		0.13		
			$\sigma$	100		0.07		
			$\sigma / <x>$	0.63		0.55		

1065  
1066 <sup>a</sup> DDHHMM indicates the start and end times (day in June 2015, hour, minute) of the data segment

1067 <sup>b</sup> Pearson product moment for the  $N_{UHSAS}(D=0.120 \mu\text{m})$  on  $V_{UHSAS}(D=0.120 \mu\text{m})$  correlation

1068 <sup>c</sup> Data recording ended at DDHHMM = 080646, i.e., 14 min before the stated end time

Formatted: Font: (Default) Times New Roman, 12 pt

Deleted: Eq. (2) and (4)

Formatted: Font: 12 pt

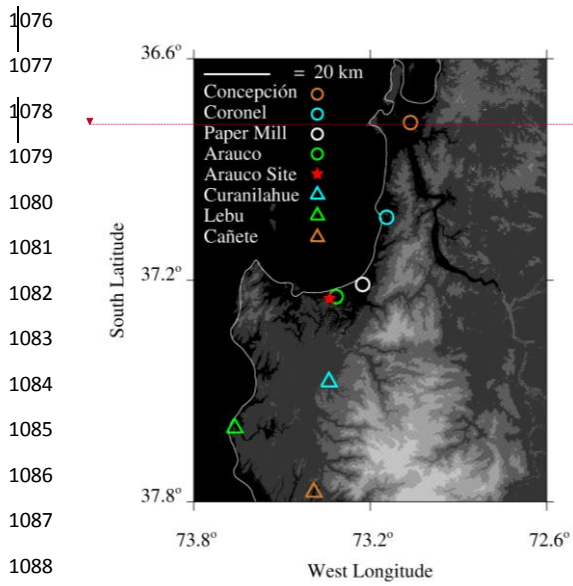
Deleted: <sup>c</sup>

Deleted: <sup>d</sup>

Deleted: ¶

<sup>c</sup> Pearson product moment for the  $N_{UHSAS}(D=0.120 \mu\text{m})$  on  $N_{CFC}$  correlation

Deleted: <sup>d</sup>



Deleted: <object>

Fig. 1 – Central Chilean Coastal region and the location of Arauco Site where aerosol measurements were made during CCOPE. Altitude thresholds for the digital elevation map are at 0 m MSL, 50 m MSL, 250 m MSL, 500 m MSL, 750 m MSL, and 1000 m MSL.

1097

1098

1099

1100

1101

1102

1103

1104

1105

1106

1107

1108

1109

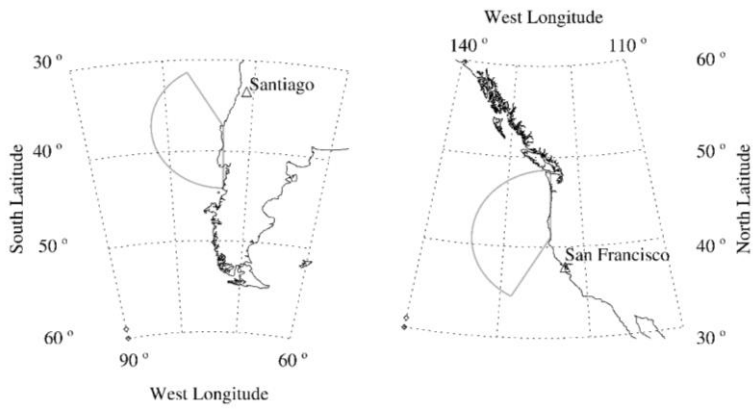


Fig. 2 - Clean sector chosen for Arauco (left, 180° to 330°) and the clean sector chosen for THD (right, 210° to 360°).

1110

1111

1112

1113

1114

1115

1116

1117

1118

1119

1120

1121

1122

1123

1124

1125

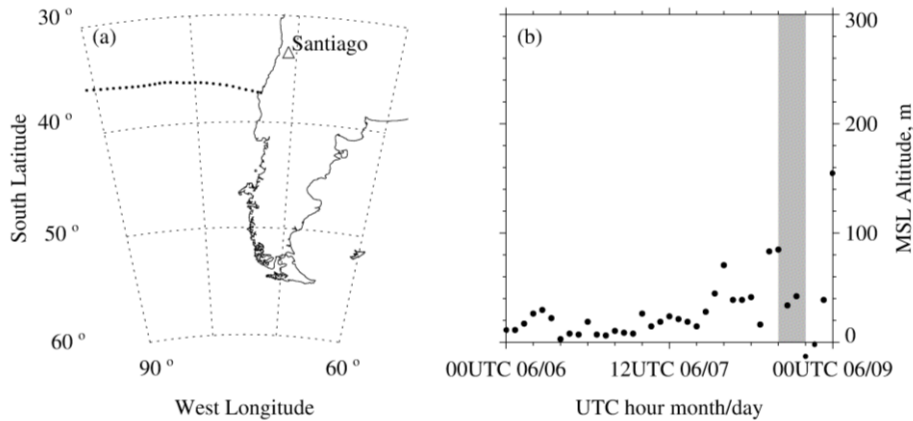
1126

1127

1128

1129

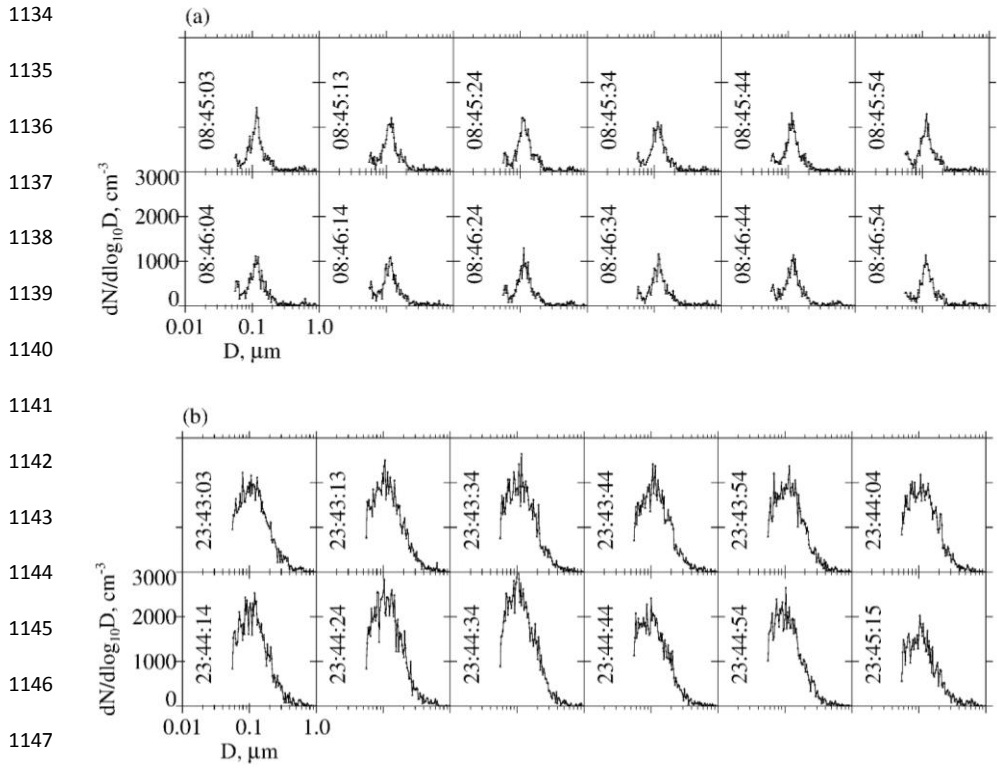
1130



Deleted: ¶

Fig. 3 - a) One of the 18 sea surface trajectories that arrived at the Arauco Site between 29 May to 28 June; this trajectory arrival occurred at 00 UTC June 9. Black dots are hourly output of the HYSPLIT model; however, for clarity, only every other 1-hr point is plotted. b) Hourly parcel MSL altitude, vs time; however, for clarity, only every other 1-hr point is plotted. The averaged sea surface wind speed ( $U$ ) was evaluated over the 12 to 18 UTC interval shown in gray. MSL altitude was calculated using the pressure output by HYSPLIT (parcel barometric pressure) and the ICAO equation for the Standard Atmosphere (1993). MSL altitude increases if a larger sea-level is pressure applied in the ICAO equation. This sensitivity is  $\sim 8 \text{ m / hPa}$ .

Deleted: HYSPLIT pressure



1150 Fig. 4 - Consecutive ASDs recorded by the UHSAS at the Arauco Site. a) ASDs with a  
 1151 relatively small concentration ( $\sim 300 \text{ cm}^{-3}$ ), a right tail of an Aitken mode (at  $\sim 0.06 \mu\text{m}$ ), and  
 1152 an accumulation mode (at  $\sim 0.1 \mu\text{m}$ ), in onshore-moving air on June 5, 2015. b) ASDs with a  
 1153 proportionately larger concentration ( $\sim 1100 \text{ cm}^{-3}$ ), an accumulation mode (at  $\sim 0.1 \mu\text{m}$ ), and no  
 1154 evidence of an Aitken mode, in air thought to be contaminated by continental sources (June 4,  
 1155 2015). UTC time is written in each panel.



1157  
1158  
1159  
1160  
1161  
1162  
1163  
1164  
1165  
1166  
1167  
1168  
1169  
1170  
1171  
1172  
1173

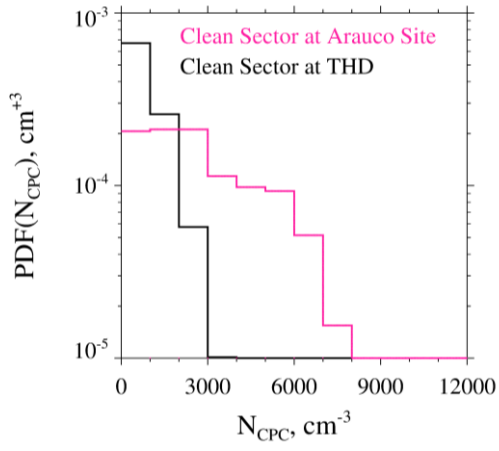
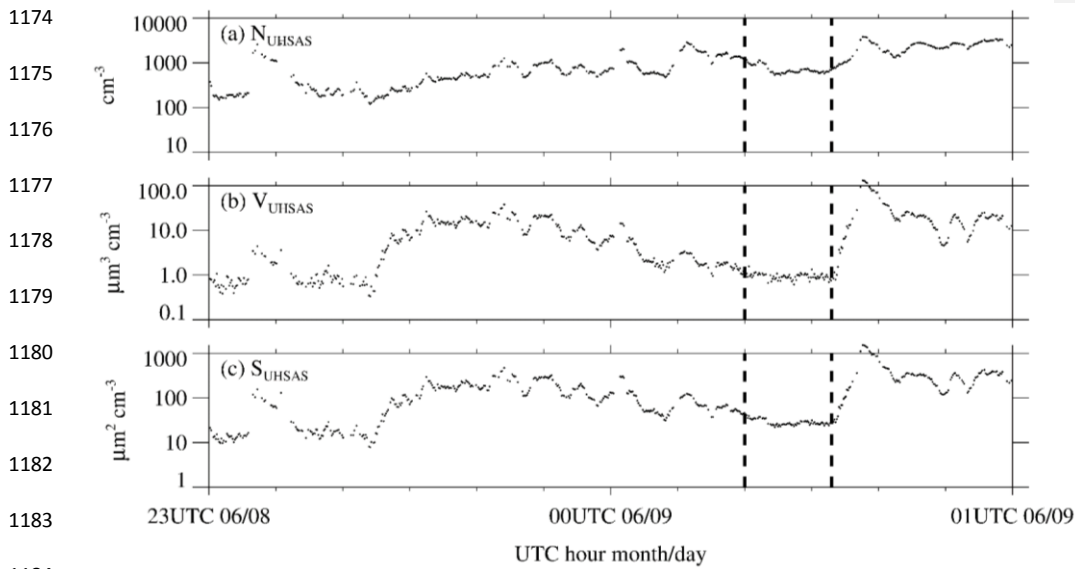
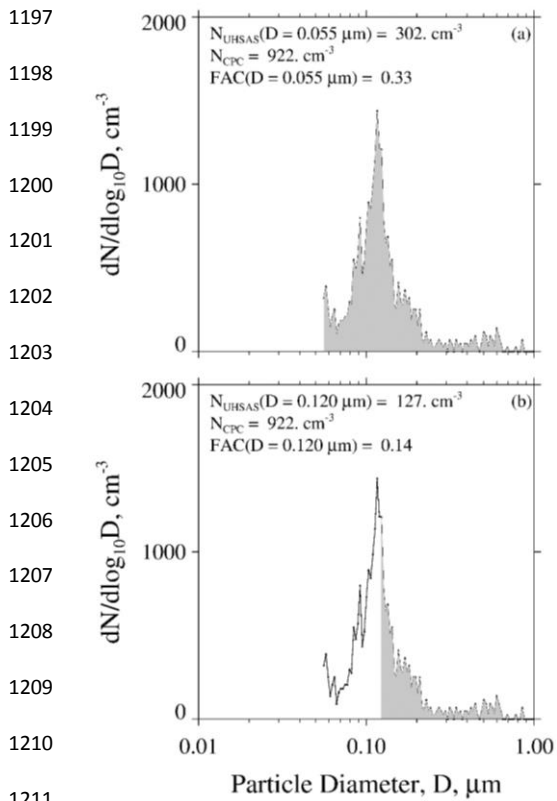


Fig. 5 - CPC concentration probability distribution functions for the Arauco Site and the

THD.



1174  
 1175  
 1176  
 1177  
 1178  
 1179  
 1180  
 1181  
 1182  
 1183  
 1184  
 1185  
 1186  
 1187  
 1188  
 1189  
 1190 Fig. 6 – Aerosol properties centered on one of the 20 onshore trajectories that arrived at  
 1191 the Arauco Site between 29 May to 28 June. This trajectory arrival occurred at 00 UTC on June  
 1192 9. a) UHSAS concentration; b) UHSAS aerosol volume; c) UHSAS aerosol surface area. Aerosol  
 1193 properties shown here were filtered using the procedure described in Appendix B. Vertical  
 1194 dashed lines mark the subset of the two-hour segment we picked (subjectively) as being  
 1195 representative of onshore-moving air that was relatively unaffected by continental aerosols  
 1196 compared to adjacent portions of the two-hour segment.



1213 Fig. 7 - Two portrayals of the ASD recorded during CCOPE at 08:45:03 UTC June 5,  
 1214 2015. This ASD is also plotted in Fig. 4a. Gray area in both panels represents the aerosol  
 1215 concentration integrated from the indicated lower-limit  $D$  to  $1 \mu\text{m}$ . a) Figure legend has the size-  
 1216 integrated UHSAS concentration, calculated with lower-limit  $D$  set at  $0.055 \mu\text{m}$ , the CPC  
 1217 concentration, and the fractional aerosol concentration ( $FAC$ ). b) Figure legend has the size-  
 1218 integrated UHSAS concentration, calculated with lower-limit  $D$  in Eq. 2 set at  $0.120 \mu\text{m}$ , the  
 1219 CPC concentration, and the fractional aerosol concentration ( $FAC$ ).

1220

1221

1222

1223

1224

1225

1226

1227

1228

1229

1230

1231

1232

1233

1234

1235

1236

1237

1238

1239

1240

1241

1242

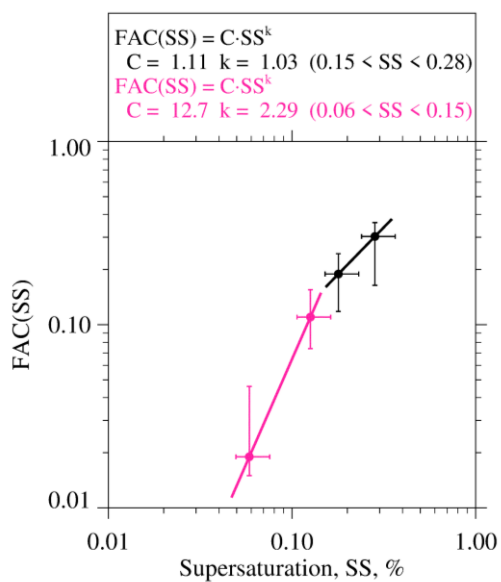
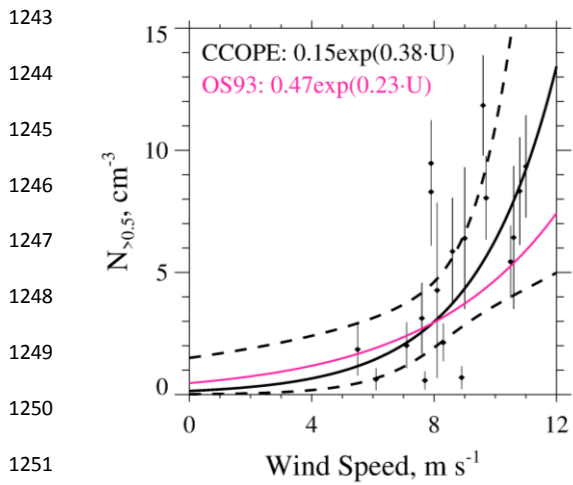
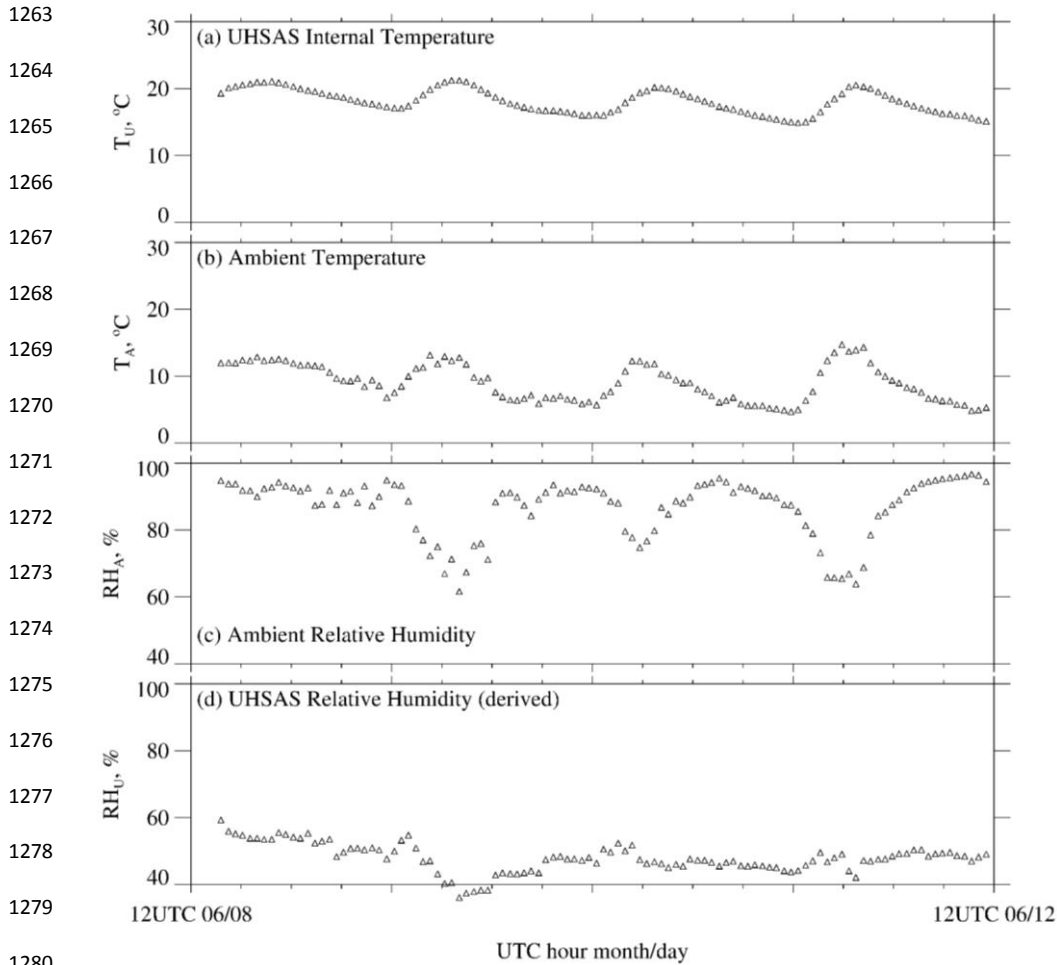


Fig. 8 - Parameterized CCN activity spectrum derived using CPC and UHSAS

measurements from the 20 onshore trajectories that arrived at the Arauco Site between 29 May and 28 June 2015. Pink circles and the pink fit line are for lower-limit diameters set at 0.200 and 0.120  $\mu\text{m}$ . Black circles and the black fit line are for lower-limit diameters set at 0.095 and 0.070  $\mu\text{m}$ . Figure legend has power-law coefficients describing the parameterization; i.e., how *FAC* varies with *SS*.

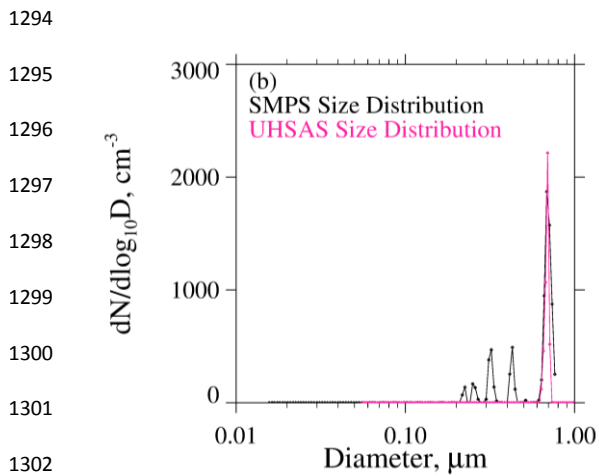
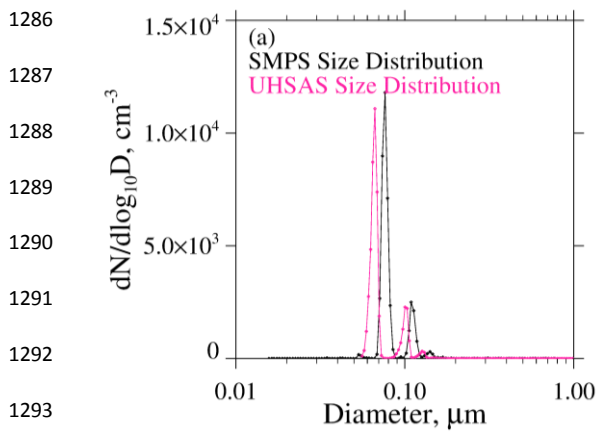


1257 Fig. 9 – Averaged values of  $N_{>0.5}$  ( $\pm 1$  standard deviation) vs HYSPLIT-derived averaged  
 1258  $U_s$  for the 18 sea surface trajectories that arrived at the Arauco Site between 29 May and 28 June  
 1259 2015. The black curve is the fit of the CCOPE data; dashed curves above and below the black  
 1260 curves are 95% confidence intervals (Romano 1977; his Eq. 4.2.3.f). The pink curve is the fit  
 1261 reported by O’Dowd and Smith (1993) for  $0.38 \mu\text{m} < D < 0.84 \mu\text{m}$ .  
 1262

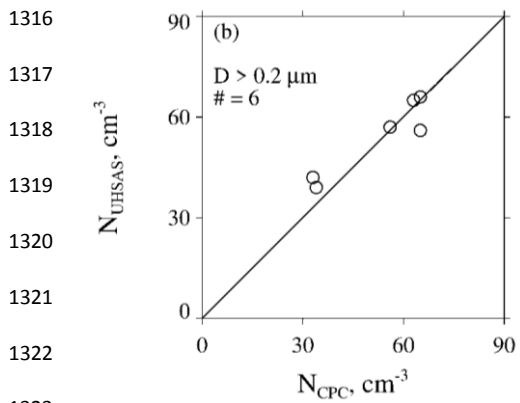
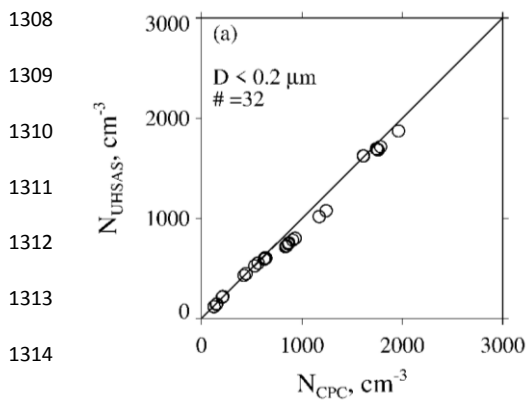


1281 Fig. A1 – UHSAS internal temperature and ambient meteorological parameters at the  
 1282 Arauco Site over a four day period. a) Temperature inside the UHSAS; b) Temperature measured  
 1283 on the meteorological tower; c)  $RH$  measured on the meteorological tower; d) Derived  $RH$  inside  
 1284 UHSAS.

1285



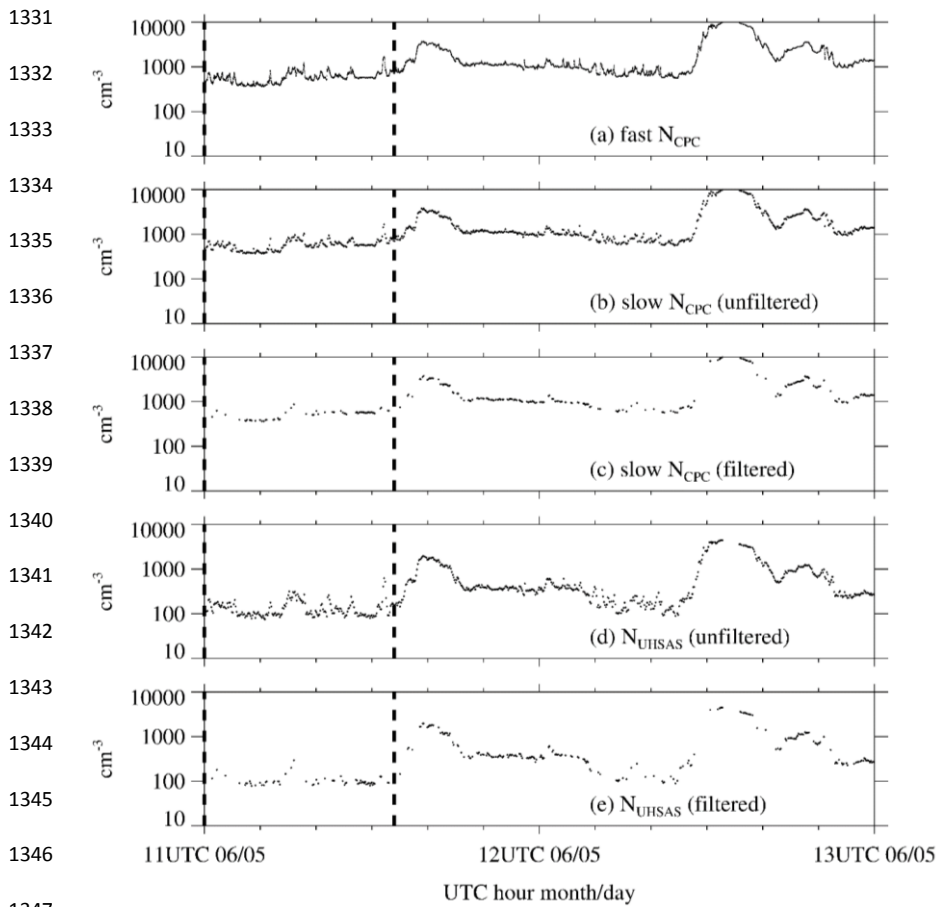
1303  
1304 Fig. A2 – a) ASDs corresponding to mobility-selected  $D = 0.075 \mu\text{m}$  ammonium sulfate  
1305 test particles. b) ASDs corresponding to mobility-selected  $D = 0.71 \mu\text{m}$  polystyrene test  
1306 particles.  
1307



1325 Fig. A3 - a) Size-integrated concentration from by the UHSAS versus concurrent  
 1326 laboratory measurements of concentration from the CPC. Results are for mobility-selected  
 1327 ammonium sulfate test particles with  $D < 0.2 \mu\text{m}$ . b) As in Fig. A3a but for mobility-selected  
 1328 ammonium sulfate test particles with  $D > 0.2 \mu\text{m}$ , and for mobility-selected polystyrene latex test  
 1329 particles with  $D > 0.2 \mu\text{m}$ .

1330





1348 Fig. B1 - Demonstration of the numerical filter. Measurements from one of the 20  
 1349 onshore trajectories that arrived at the Arauco Site between 29 May and 28 June. This trajectory  
 1350 arrival occurred at 12Z June 5. a) 1-s sampled CPC measurements; b) 10-s sampled CPC  
 1351 measurements; c) filtered 10-s CPC measurements; d) 10-s UHSAS measurements of size-  
 1352 integrated concentration; e) filtered 10-s UHSAS measurements of size-integrated concentration.  
 1353